Electronic Supplementary Material (ESI) for Materials Advances.

Supporting information for:

Luminescent molecular switches based on dicationic P-doped Polycyclic Aromatic Hydrocarbons

Table of Content

All experiments were performed under an atmosphere of dry argon using standard Schlenk techniques. Commercially available reagents were used as received without further purification. Solvents were freshly purified using MBRAUN SPS-800 drying columns. Separations were performed by gravity column chromatography on basic alumina (Aldrich, Type 5016A, 150 mesh, 58 Å) or silica gel (Merck Geduran 60, 0.063-0.200 mm).^{1}H, ^{13}C, ^{19}F and ^{31}P NMR spectra were recorded on Bruker AV III 400 MHz NMR spectrometers equipped with BBFO probeheads. Assignment of H and C atoms is based on COSY, NOESY, edited-HSQC and HMBC experiments. For products **2-6**, special ^{31}P decoupled experiments ({^{31}P}^{1}H, {^{31}P-^{1}H}^{13}C, {^{31}P}-HSQC, HMBC, COSY, NOESY) were performed on a Bruker Av III HD 500 MHz fitted with a triple inverse probehead (^{1}H-^{31}P-X). These ^{31}P decoupled experiments have been performed using the PRISM core facility (Biogenouest©, UMS Biosit, Université de Rennes 1- Campus de Villejean- 35043 RENNES Cedex, FRANCE). ^{1}H and ^{13}C NMR chemical shifts were reported in parts per million (ppm) using residual solvent signal as reference. High-resolution mass spectra were obtained on a Varian MAT 311 or ZabSpec TOF Micromass instrument at Scanmat (UMS 2001). UV-Visible spectra were recorded at room temperature on a VARIAN Cary 5000 spectrophotometer. The UV-Vis emission and excitation spectra measurements were recorded on a FL 920 Edimburgh Instrument equipped with a Hamamatsu R5509-73 photomultiplier for the NIR domain (300-1700 nm) and corrected for the response of the photomultiplier. The absolute quantum yields (AQYs) were measured with a C9920-03 Hamamatsu system equipped with a150 W xenon lamp, a monochromator, an integrating sphere. The electrochemical studies were carried out under argon using an Eco ChemieAutolab PGSTAT 30 potentiostat for cyclic voltammetry with the three-electrode configuration: the working electrode was a platinum disk, the reference electrode was a saturated calomel electrode and the counter-electrode a platinum wire. All potential were internally referenced to the ferrocene/ ferrocenium couple. For the measurements, concentrations of 10^{-3} M of the electroactive species were used in freshly distilled and degassed dichloromethane and 0.2 M tetrabutylammoniumhexafluorophosphate. The spectroelectrochemical setup was performed in DCM, -[NBu$_4$][PF$_6$] 0.2 M using a Pt grid as the working electrode, a Pt wire as the counter electrode and SCE reference electrode. A Shimatzu 3600 spectrophotometer was employed to record the UV-vis-NIR spectra. The EPR measurements were performed on a Brucker ESP-300E X-band spectrometer. Synthesis of **2**[OTf], **4a**[OTf]$_2$ and **5-8**[OTf]$_2$were prepared according to the literature.[1]

[1] Q. Ge, J. Zong, B. Li and B. Wang, *Org. Lett.*, 2017, **19**, 6670-6673; T. Delouche, A. Vacher, E. Caytan, T. Roisnel, B. Le Guennic, D. Jacquemin, M. Hissler and P.-A. Bouit, *Chem. Eur. J.*, DOI: 10.1002/chem.202001213.

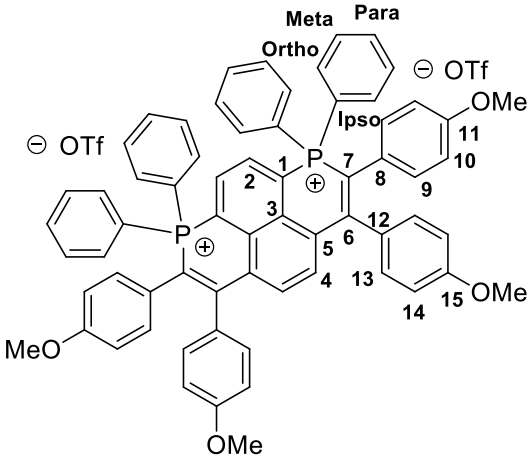

4c$[OTf]_2$: (**General method A**) 1,4-bis(diphenylphosphino)naphtalene (95 mg, 0.192 mmol, 1 eq), Bis-(4-methoxyphenyl)acetylene (110 mg, 0.462 mmol, 2.4 eq) and $Cu(OTf)_2$ (278 mg, 0.709 mmol, 4 eq) were dissolved in 16 mL of degazed acetonitrile. The mixture was heated at 100°C overnight. The solvent was evaporated and the crude mixture was purified on silica gel chromatography. (DCM/Acetone : 7/3). An orange powder was obtained (178 mg, η = 73 %). **^{1}H NMR** (400 MHz, CD_2Cl_2) δ 8.44 – 8.33 (m, 2H, H_2), 7.86 – 7.77 (m, 12H, $H_{ortho,\ para}$), 7.71 (s, 2H, H_4), 7.70 – 7.63 (m, 8H, H_{meta}), 7.22 (d, *J* = 8.7 Hz, 4H, H_{13}), 6.83 (d, *J* = 8.8 Hz, 4H, H_{14}), 6.68 – 6.60 (d, *J* = 8.9 Hz, 4H, H_9), 6.56 – 6.47 (d, *J* = 8.8 Hz, 4H, H_{10}), 3.75 (s, 6H, $H_{\text{-OMe}}$), 3.63 (s, 6H, $H_{\text{-OMe}}$). **^{13}C NMR** (101 MHz, , CD_2Cl_2) δ 160.29 (Cq), 160.10 (Cq), 136.53 (C_4), 135.97 (C_2), 135.0 (d, *J* = 11.4 Hz, C_{ortho}), 135.0 (Cq), 133.38 (d, *J* = 14.5 Hz, Cq), 132.44 (d, *J* = 4.0 Hz, C_9), 131.94 (C_{13}), 131.00 (d, *J* = 13.8 Hz, C_{meta}), 131.00 (C_{para}) 129.76 (Cq), 128.70 (d, *J* = 14.3 Hz, Cq), 124.46 (Cq), 122.80 (d, *J* = 16.4 Hz, Cq), 118.63 (d, *J* = 92.9 Hz, C_{ipso}), 117.86 (d, *J* = 75.8 Hz, Cq), 114.34 (s, C_{10}), 114.26 (s, C_{14}) 55.67 ($C_{\text{-OMe}}$), 55.54 ($C_{\text{-OMe}}$). C_{OTf} is not observed due to overlap. **^{19}F NMR** (376 MHz, CD_2Cl_2): δ -78.8. **^{31}P NMR** (162 MHz, CD_2Cl_2) δ +1.1. **HRMS** (ESI, CH_3OH / CH_2Cl_2 : 90/10) $C^{++}(C_{66}H_{52}O_4P_2)$: m/z Theoretical : 485.1665, m/z Found : 485.1687.

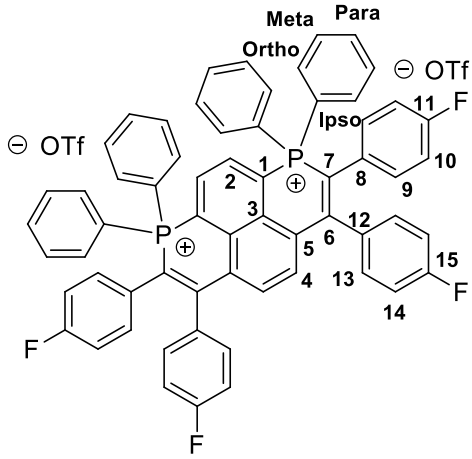

4d$[OTf]_2$:**General method A** was used with the 1,4-bis(diphenylphosphino)naphtalene (80 mg, 0.16 mmol, 1 eq), Bis-(4-fluorophenyl)acetylene (83 mg, 0.39 mmol, 2.4 eq) and $Cu(OTf)_2$ (234 mg, 0.65 mmol, 4 eq). The crude mixture is purified on silica gel chromatography (DCM/Acetone : 1/1). A yellow powder was obtained (153 mg, η = 78 %). **^{1}H NMR** (400 MHz, CD_2Cl_2) δ 8.38 – 8.31 (m, 2H, H_2), 7.91 – 7.84 (m, 8H, H_{ortho}), 7.83 – 7.78 (m, 4H, H_{para}), 7.72 – 7.67 (m, 8H, H_{meta}), 7.66 (s, 2H, H_4), 7.39 – 7.34 (m, 4H, H_{13}), 7.00 (t, *J* = 8.5 Hz, 4H, H_{14}), 6.76 – 6.69 (m, 8H, $H_{9,10}$). **^{13}C NMR** (101 MHz, CD_2Cl_2) δ 164.22 (d, *J* = 14.2 Hz, Cq), 161.78 (d, *J* = 16.2 Hz, Cq), 159.9 (Cq), 136.6 (s, C_4), 136.2 (d, *J* = 1.2 Hz, C_{para}), 135.9 (d, *J* = 22.1 Hz, C_2), 135.14 (d, *J* = 11.4 Hz, C_{ortho}), 134.5 (d, *J* = 26.5 Hz, Cq), 133.3 (d, *J* = 7.1 Hz, C_9), 132.5 (d, *J* = 7.5 Hz, C_{13}), 130.9 (d, *J* = 13.9 Hz, C_{meta}), 129.8 (d, *J* = 57.9 Hz, Cq), 128.9 (d, *J* = 99.2 Hz, Cq), 122,7 (d, *J* = 31.4 Hz, Cq), 121.7 (s, Cq), 119.7 (Cq), 118.15 (d, *J* = 92.4 Hz, C_{ipso}), 116.19 (d, *J* = 21.9 Hz, C_{10}), 116.01 (d, *J* = 21.9 Hz, C_{14}). **^{19}F NMR** (376 MHz, CD_2Cl_2): δ -78.8 (s, F_{OTf}), -111.5 (d, *J* = 3.3 Hz, F_{11}), -112.2 (s, F_{15}). **^{31}P NMR** (162 MHz, CD_2Cl_2) δ +1.5. **HRMS** (ESI, CH_2Cl_2) $C^{++}(C_{62}H_{40}F_4P_2)$: m/z Theoretical : 461.1265, m/z Found : 461.1264.

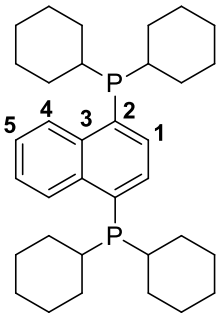

1,4-bis(dicyclohexylphosphaneyl)naphthalene: 1,4-Dibromonaphtalene (1.0 g, 3.5 mmol, 1 eq) was degassed under argon and dissolved in 50 ml of dry Et_2O. Then, the mixture was cooled to -78°C and *t*-BuLi (1.5 mL, 2,10 mmol, 3 eq) was added dropwise. After 30 min at -78 °C, the reaction was allowed to warm up to room temperature (RT). After 30 min the reaction is cooled to -78°C and PPh_2Cl (570 mg, 2.45 mmol, 3.5 eq) was added dropwise and stirred at -78°C for 30 min and then at RT overnight. Then the organic phase was extracted with water, dried over MgSO4 and the solvent evaporated. The product was purified through silica gel column chromatography (C_7/DCM : 9/1). A white powder was obtained (253 mg, η = 70 %). **^{1}H NMR** (400 MHz, CD_2Cl_2) δ 8.96 – 8.83 (m, 2H, H_5), 7.63 (s, 2H, H_1), 7.54 – 7.40 (m, 2H, H_4), 2.12 – 2.01 (m, 4H, H_{Cy}), 2.00 – 1.89 (m, 4H, H_{Cy}), 1.80 – 1.71 (m, 4H, H_{Cy}), 1.67 – 1.60 (m, 12H, H_{Cy}), 1.38 – 0.99 (m, 20H, H_{Cy}). **^{13}C NMR** (101 MHz, CD_2Cl_2) δ 138.9 (d, *J* = 21.6 Hz, Cq), 134.1 (d, *J* = 16.5 Hz, Cq), 130.2 (C_1), 127.7 (d, *J* = 44.2 Hz, Cq), 125.4 (C_5), 33.7 (d, *J* = 12.9 Hz, C_{Cy}), 31.0 (s, C_{Cy}), 30.9 (s, C_{Cy}), 29.5 (s, C_{Cy}), 29.4 (s, C_{Cy}), 27.8 (s, C_{Cy}), 27.59 (d, *J* = 5.2 Hz, C_{Cy}), 27.46 (s, C_{Cy}), 26.84 (s, C_{Cy}). One ^{13}C is missing due to overlap. **^{31}P NMR** (121 MHz, , CD_2Cl_2) δ -16.48. **HRMS** (ESI, CH_3OH / CH_2Cl_2 : 90/10) $[M+H]^+$ ($C_{34}H_{51}P_2$) : m/z Theoretical : 521.3461, m/z Found : 521.3460.

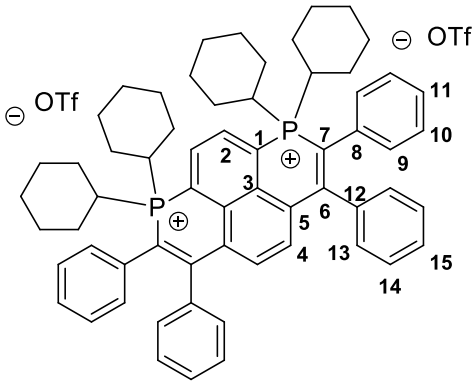

4b$[OTf]_2$: **General method B** was used with the compound DT494 (81 mg, 0.16 mmol, 1 eq), diphenylacetylene (67 mg, 0.37 mmol, 2.4 eq) and $Cu(OTf)_2$ (225 mg, 0.62 mmol, 4 eq). The crude mixture is purified on silica gel chromatography (DCM/Acétone : 8/2). A yellow powder was obtained (130 mg, η = 71 %). **^{1}H NMR** (400 MHz, CD_2Cl_2) δ 9.13 – 9.05 (m, 2H, H_2), 7.40 (s, 2H, H_4), 7.38 – 7.34 (m, 6H, $H_{9,11}$), 7.28 – 7.24 (m, 6H, $H_{13,15}$), 7.15 – 7.08 (m, 8H, $H_{10,14}$), 3.18 – 2.99 (m, 4H, H_{Cy}), 2.05 – 1.89 (m, 12H, H_{Cy}), 1.82 – 1.63 (m, 12H, H_{Cy}), 1.54 – 1.42 (m, 8H, H_{Cy}), 1.11 – 0.94 (m, 4H, H_{Cy}), 0.73 – 0.56 (m, 4H, H_{Cy}). **^{13}C NMR** (101 MHz, , CD_2Cl_2) δ 161.44 (Cq), 136.39 (d, *J* = 12.2 Hz, Cq), 135.78 (C_4), 135.45 (d, *J* = 21,5 Hz, C_2), 133.46 (d, *J* = 7.1 Hz, Cq), 132.85 (d, *J* = 10.1 Hz, Cq), 130.36 (d, *J* = 1.2 Hz, C_9), 130.05 (C_{11}), 129.9 (C_{10}), 129.8 (C_{14}), 129.19 (C_{15}), 128.93 (C_{13}), 122.97 (Cq), 119.77 (Cq), 117.1 (d, *J* = 88.9 Hz, Cq), 33.75 (d, *J* = 42.8 Hz, C_{Cy}), 26.53 (d, *J* = 13.8 Hz, C_{Cy}), 26.21 (d, *J* = 14.3 Hz, C_{Cy}), 25.86 (C_{Cy}), 25.46 (C_{Cy}), 24.99 (C_{Cy}). **^{19}F NMR** (376 MHz, CD_2Cl_2) δ -78.84. **^{31}P NMR** (162 MHz, , CD_2Cl_2) δ 12.2. **HRMS** (ESI, CH_3OH / CH_2Cl_2 : 90/10) $[C^{2+}, CF_3SO_3^-]^+$($C_{63}H_{68}O_3F_3P_2S$) : m/z Theoretical : 1023.4311, m/z Found : 1023.4306.

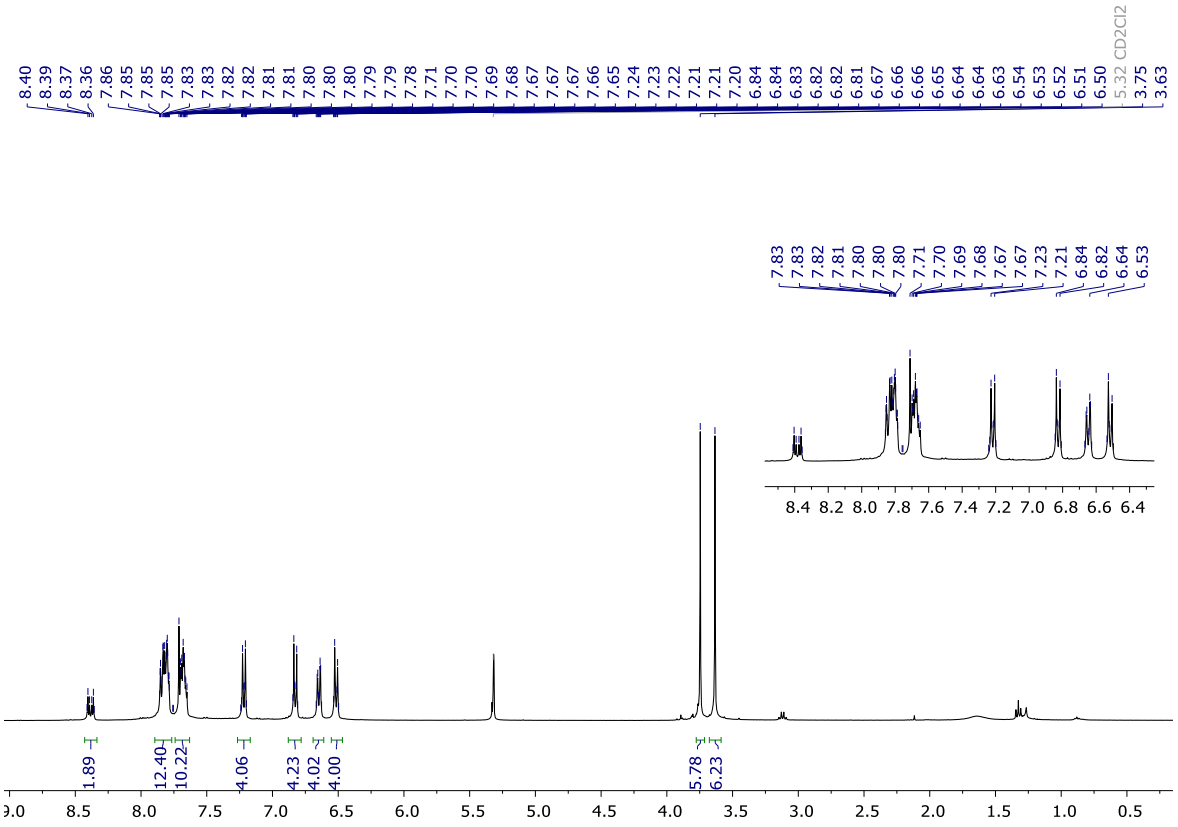

Figure **S1**: ^{1}H NMR (400 MHz, CD_2Cl_2) spectrum of **4c**$[OTf]_2$.

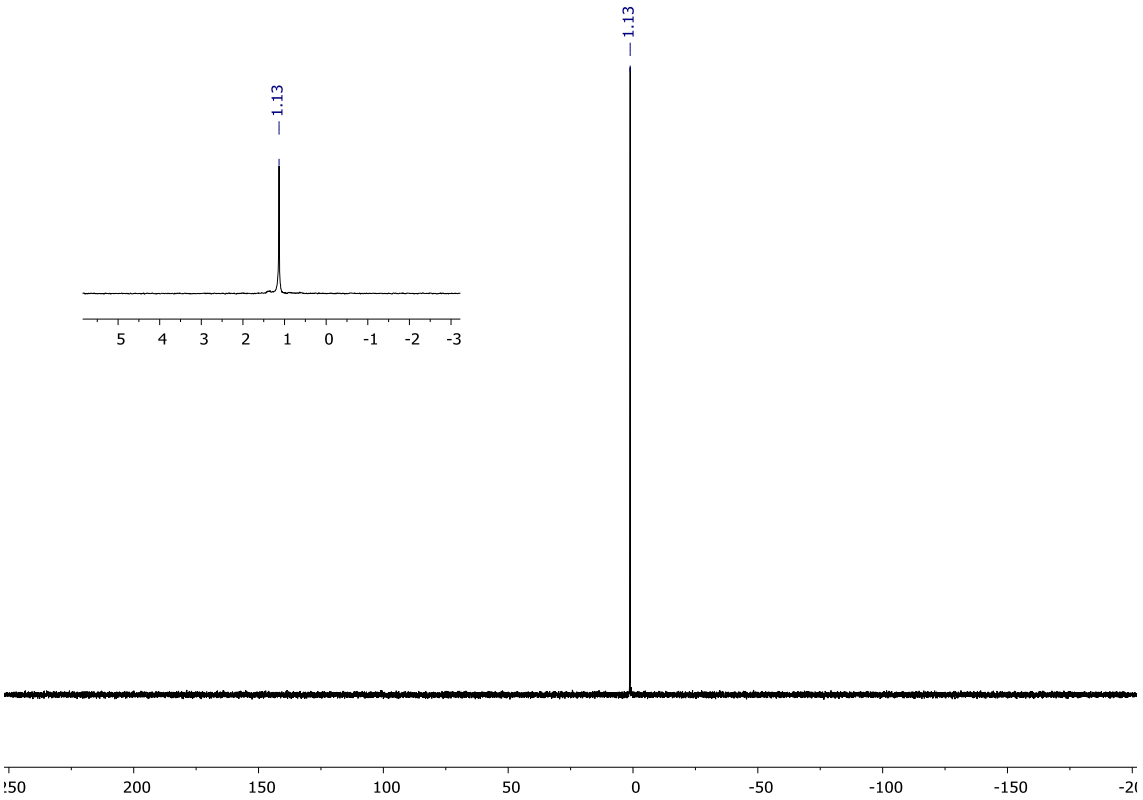

Figure **S2**: ^{31}P NMR (162 MHz, CD_2Cl_2) spectrum of **4c**$[OTf]_2$.

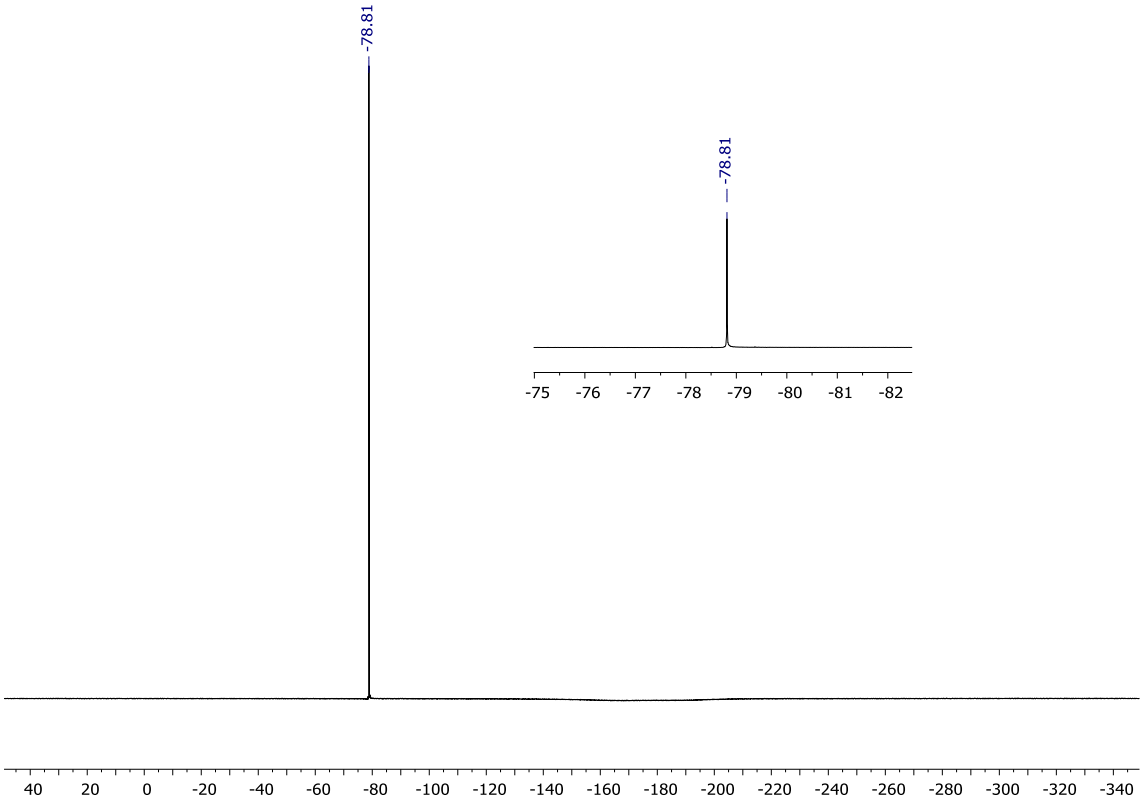

Figure **S3**: ^{19}F NMR (376 MHz, CD_2Cl_2) spectrum of **4c**$[OTf]_2$.

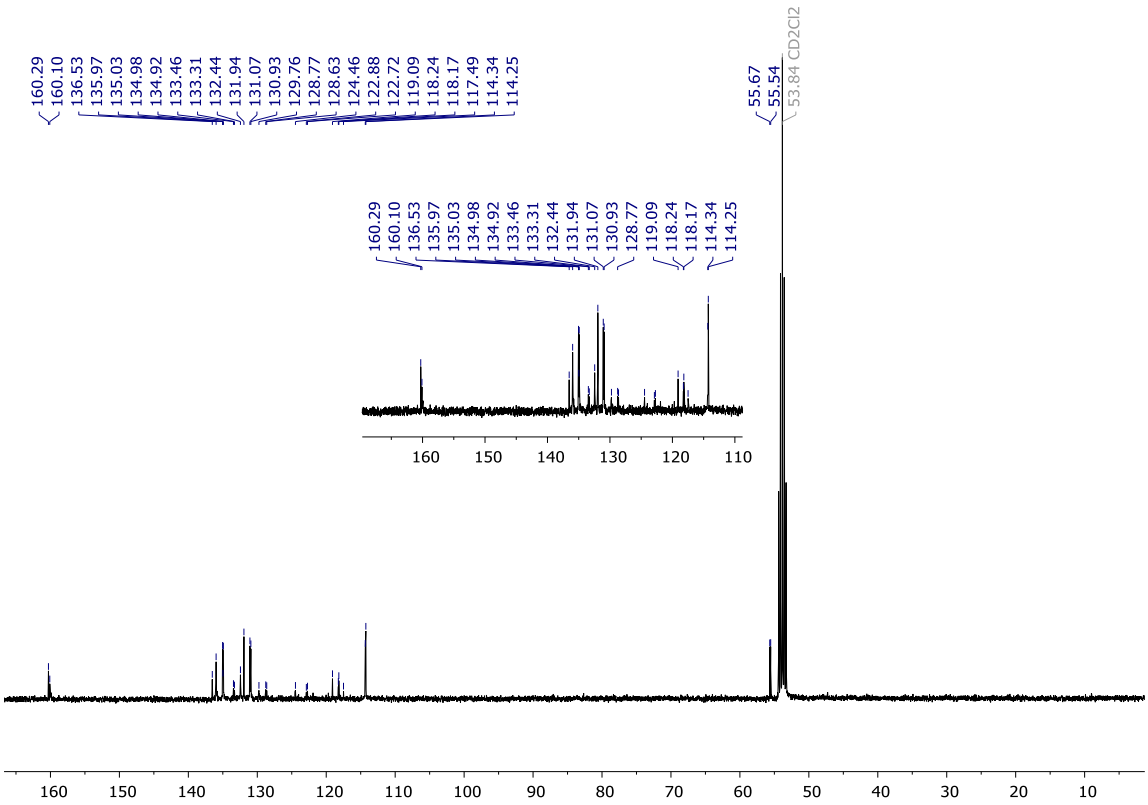

Figure **S4**: ^{13}CNMR (101 MHz, CD_2Cl_2) spectrum of **4c**$[OTf]_2$.

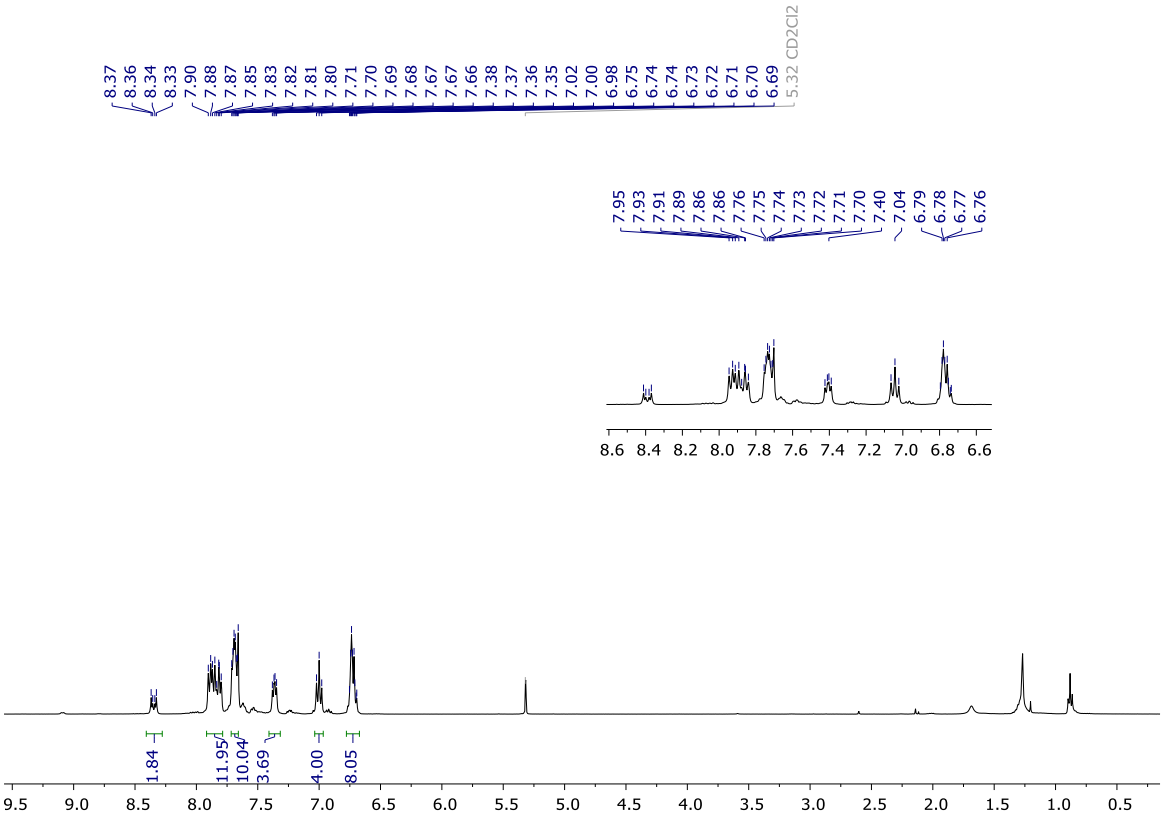

Figure **S5**: ^{1}H NMR (400 MHz, CD_2Cl_2) spectrum of **4d**$[OTf]_2$.

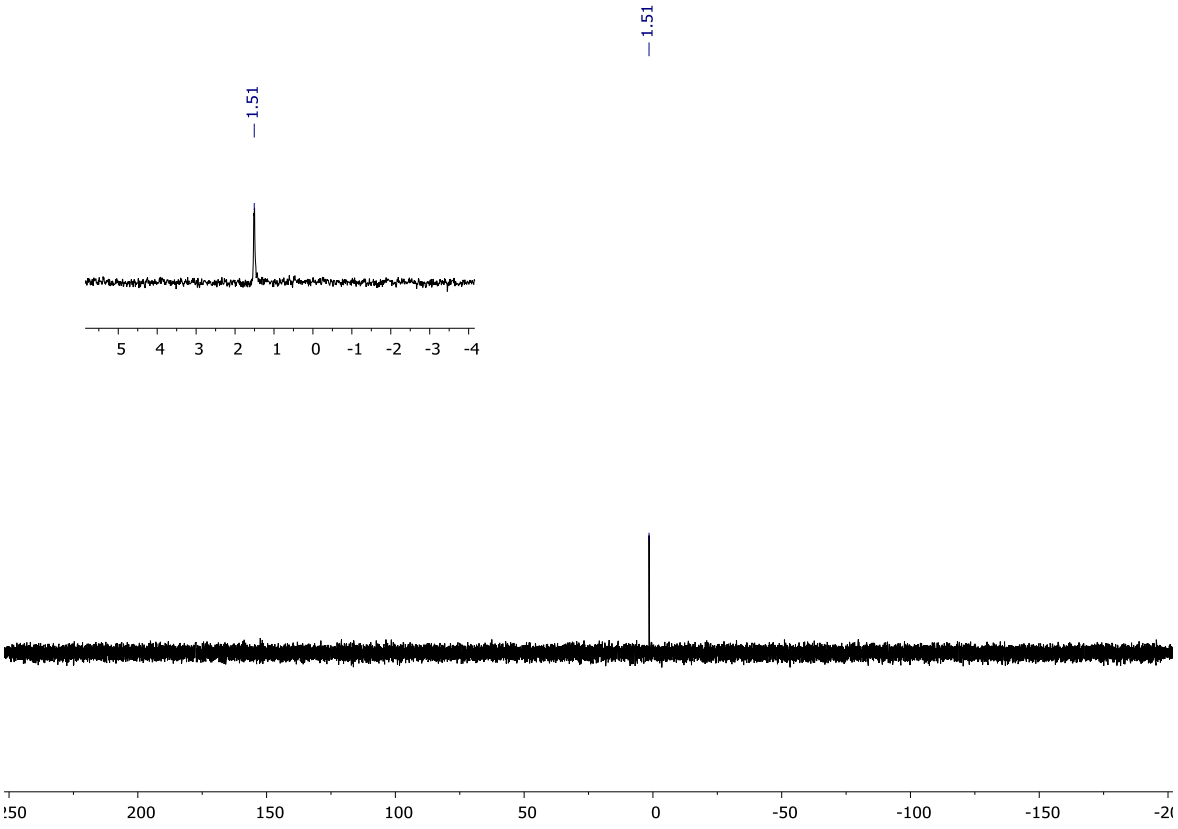

Figure **S6**: ^{31}P NMR (162 MHz, CD_2Cl_2) spectrum of **4d**$[OTf]_2$.

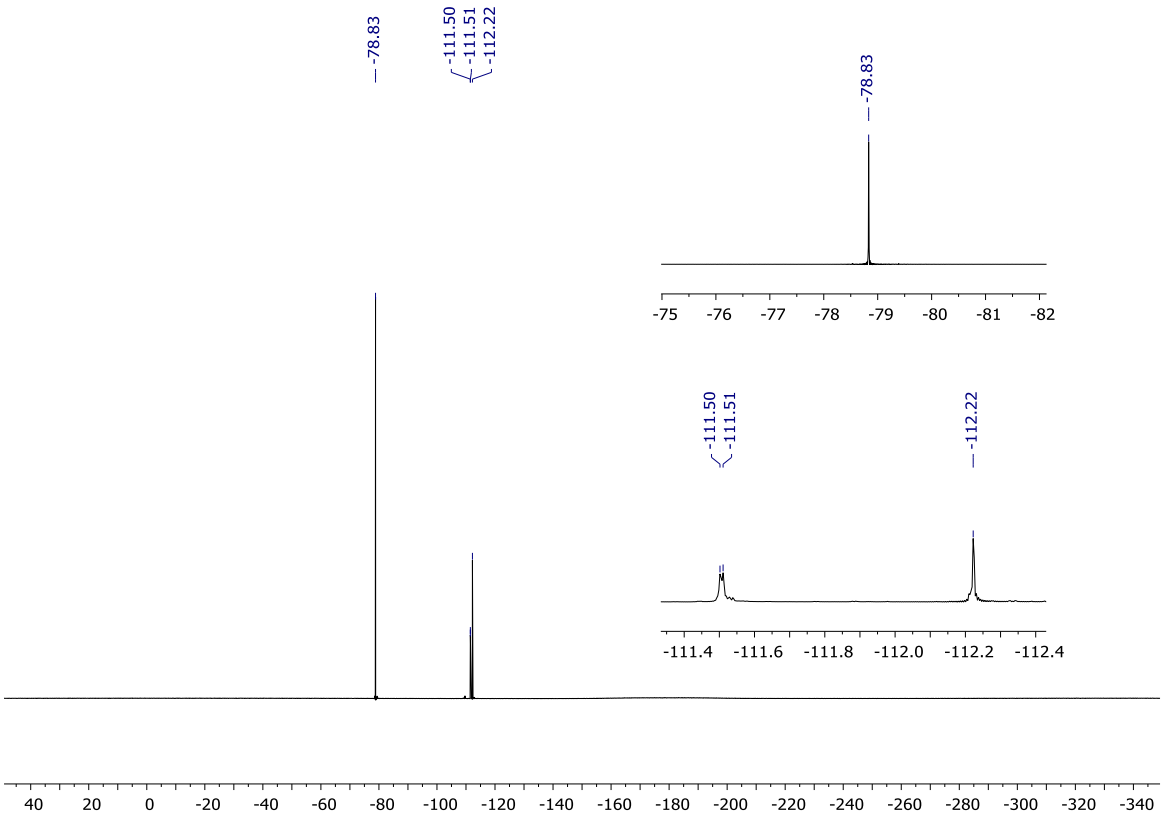

Figure **S7**: ^{19}F NMR (376 MHz, CD_2Cl_2) spectrum of **4d**$[OTf]_2$.

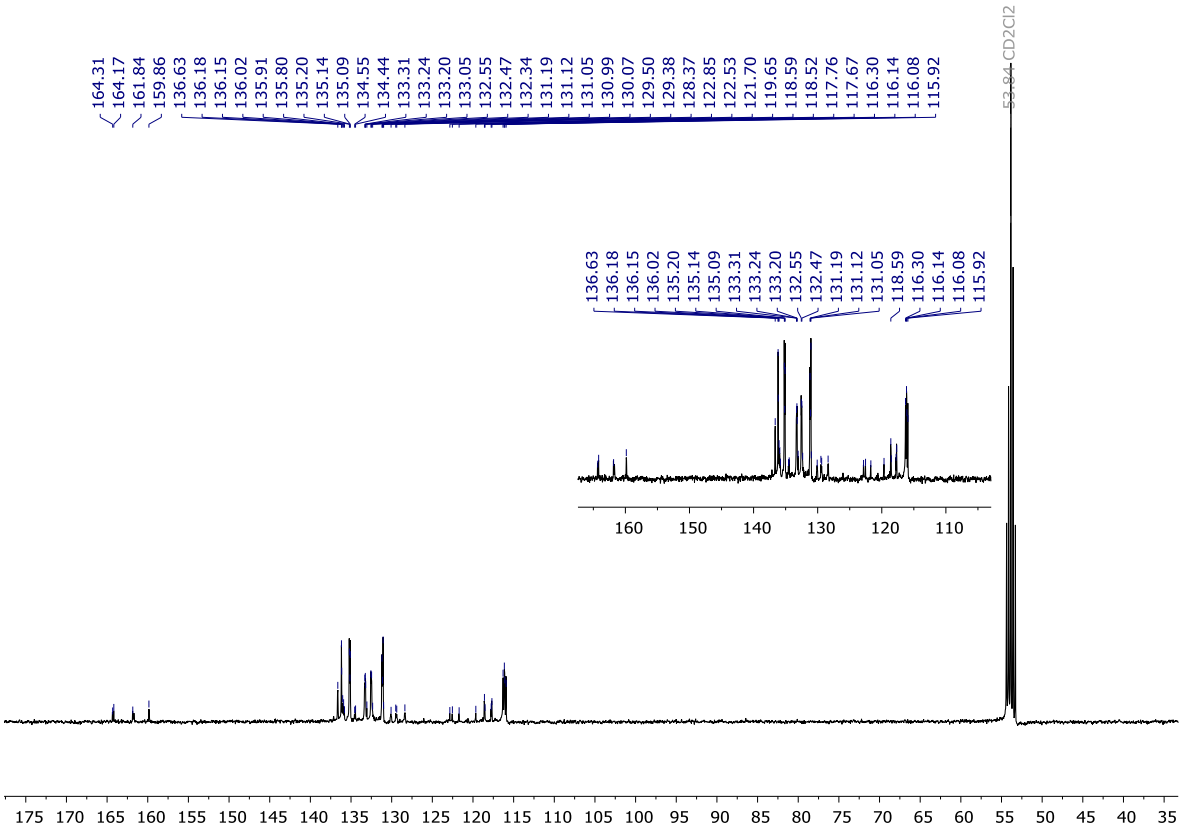

Figure **S8**: ^{13}C NMR (101 MHz, CD_2Cl_2) spectrum of **4d**$[OTf]_2$.

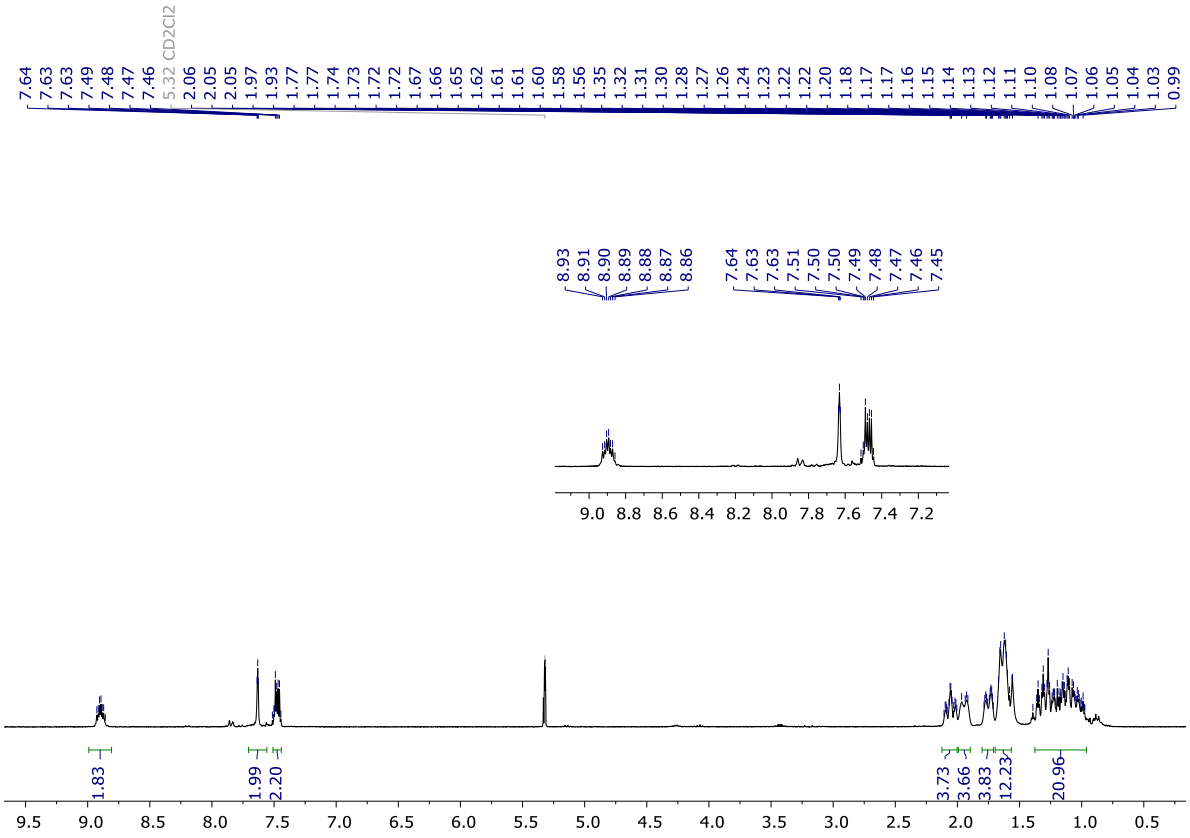

Figure **S9**: ^{1}H NMR (300 MHz, CD_2Cl_2) spectrum of 1,4-bis(dicyclohexylphosphaneyl)naphthalene.

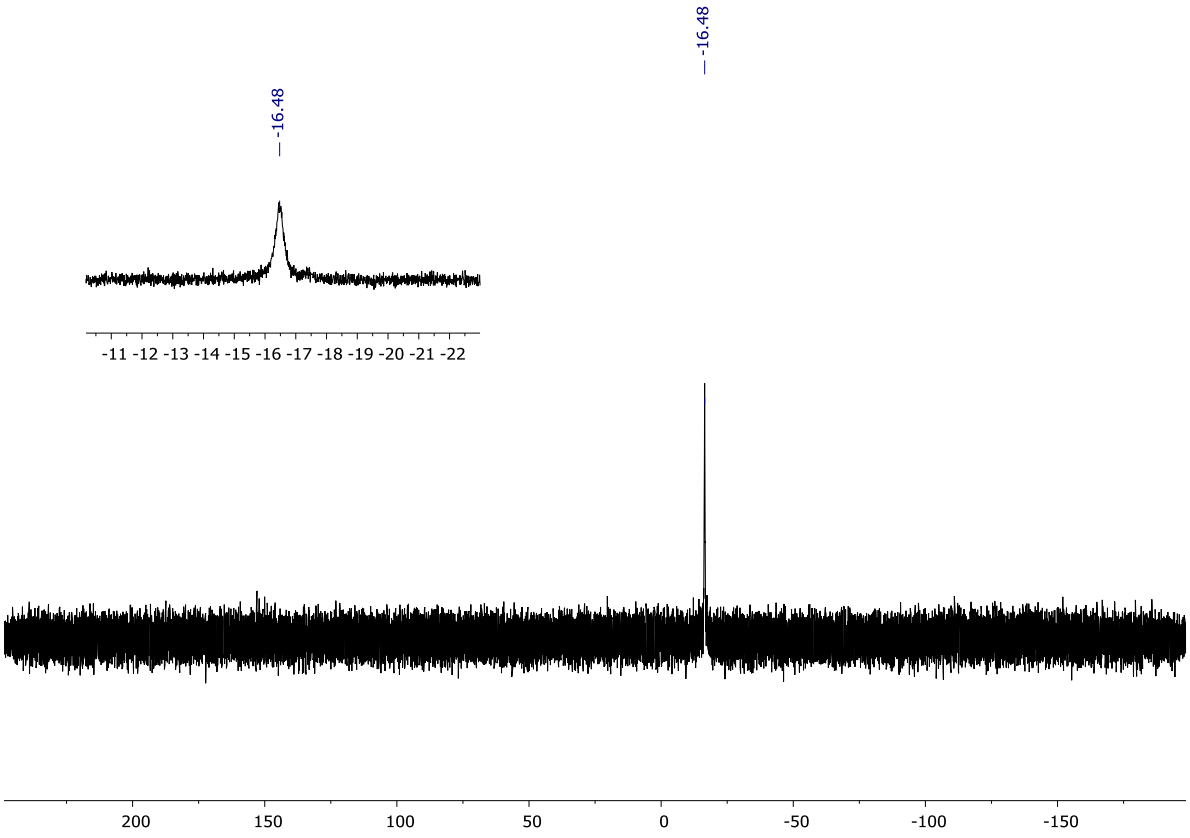

Figure **S10**: ^{31}P NMR (121 MHz, CD_2Cl_2) spectrum of 1,4-bis(dicyclohexylphosphaneyl)naphthalene.

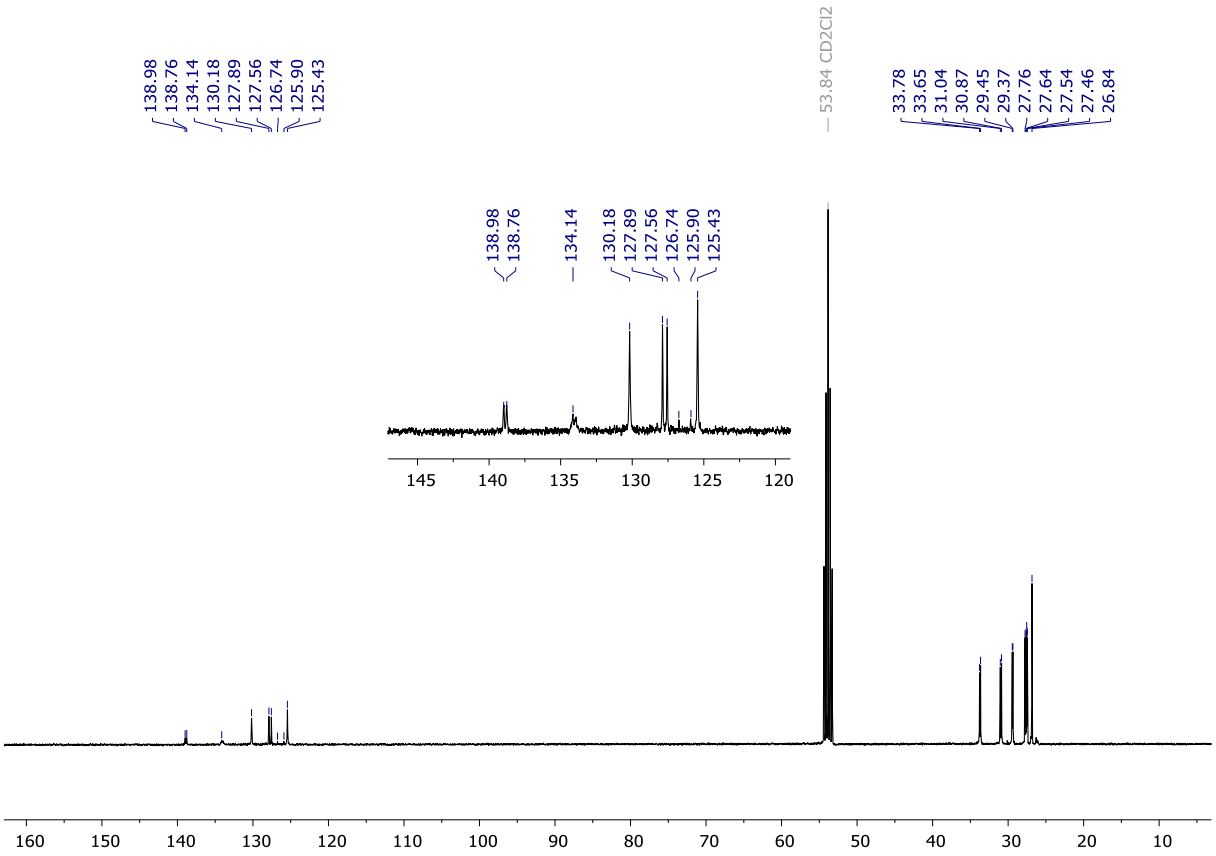

Figure **S11**: ^{13}C NMR (101 MHz, CD_2Cl_2) spectrum of 1,4-bis(dicyclohexylphosphaneyl)naphthalene

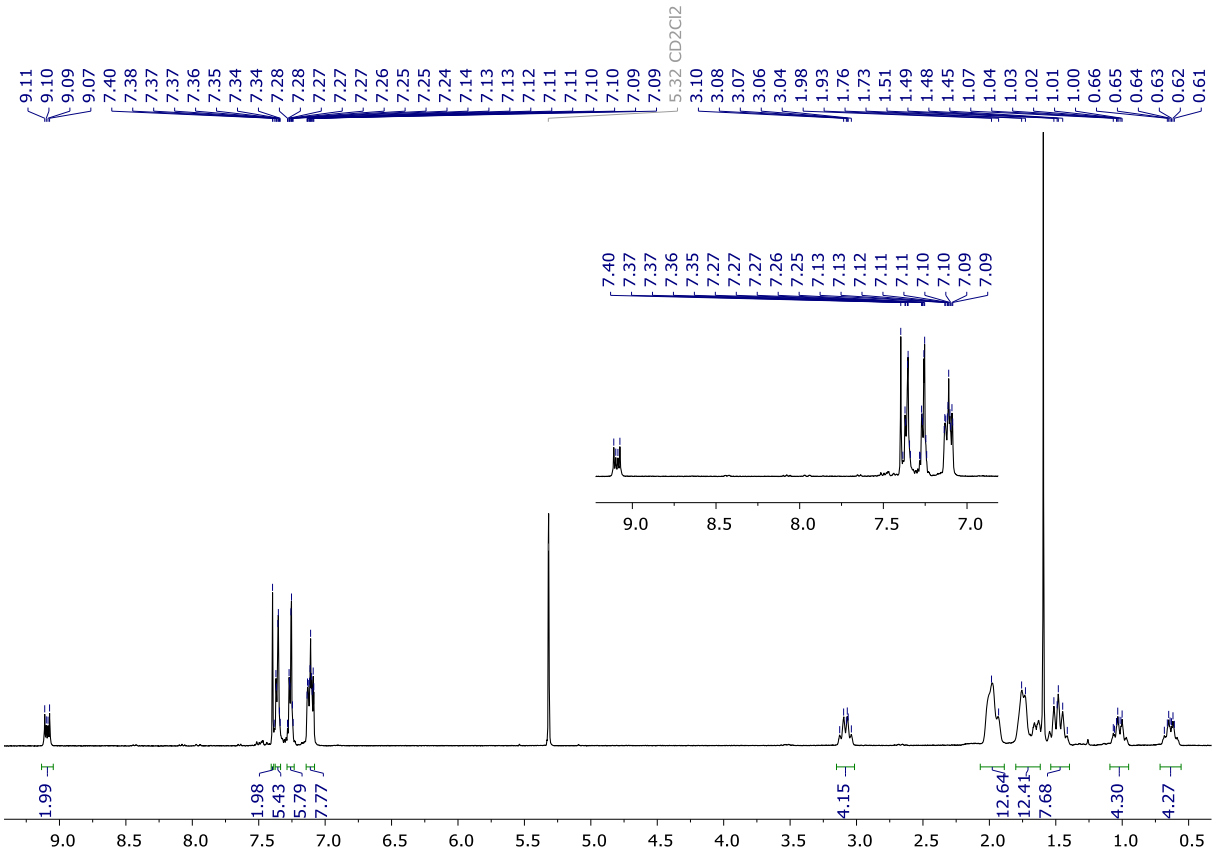

Figure **S12**: ^{1}H NMR (400 MHz, CD_2Cl_2) spectrum of **4b**[OTf]$_2$.

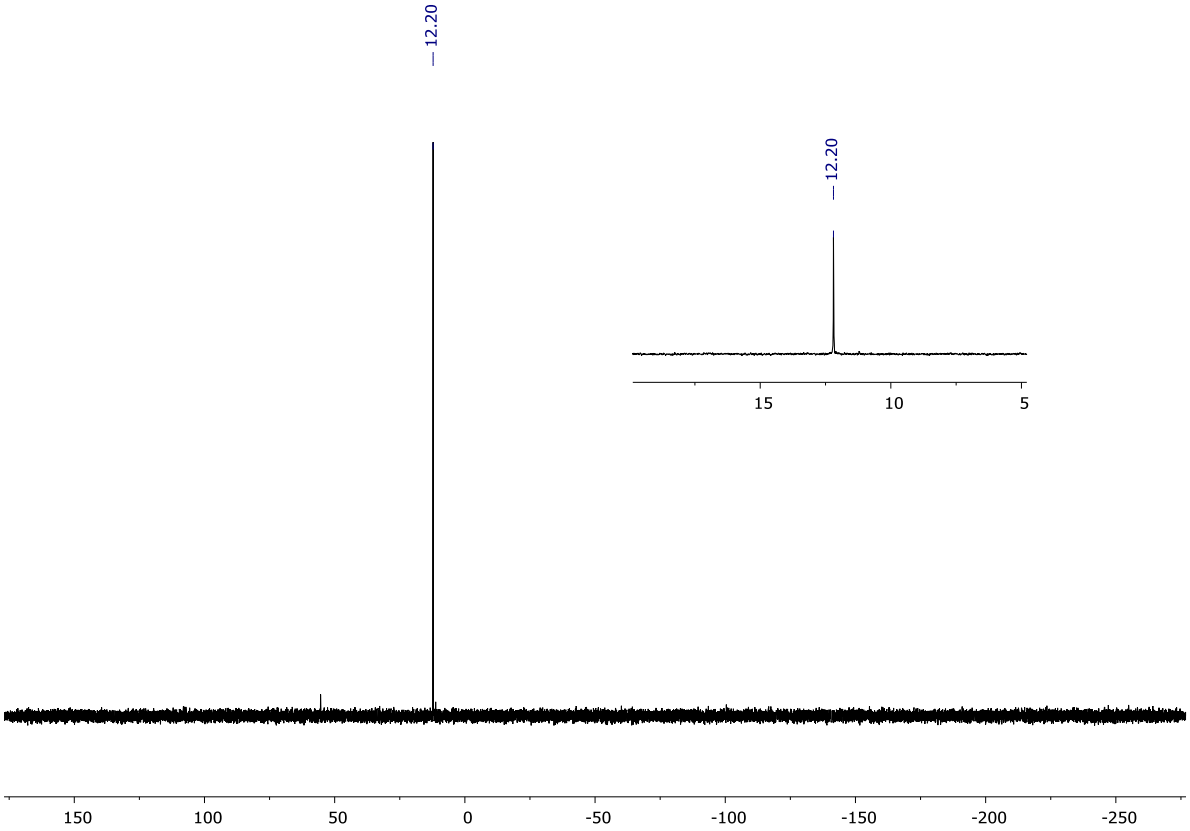

Figure **S13**: ^{31}P NMR (162 MHz, CD_2Cl_2) spectrum of **4b**[OTf]$_2$.

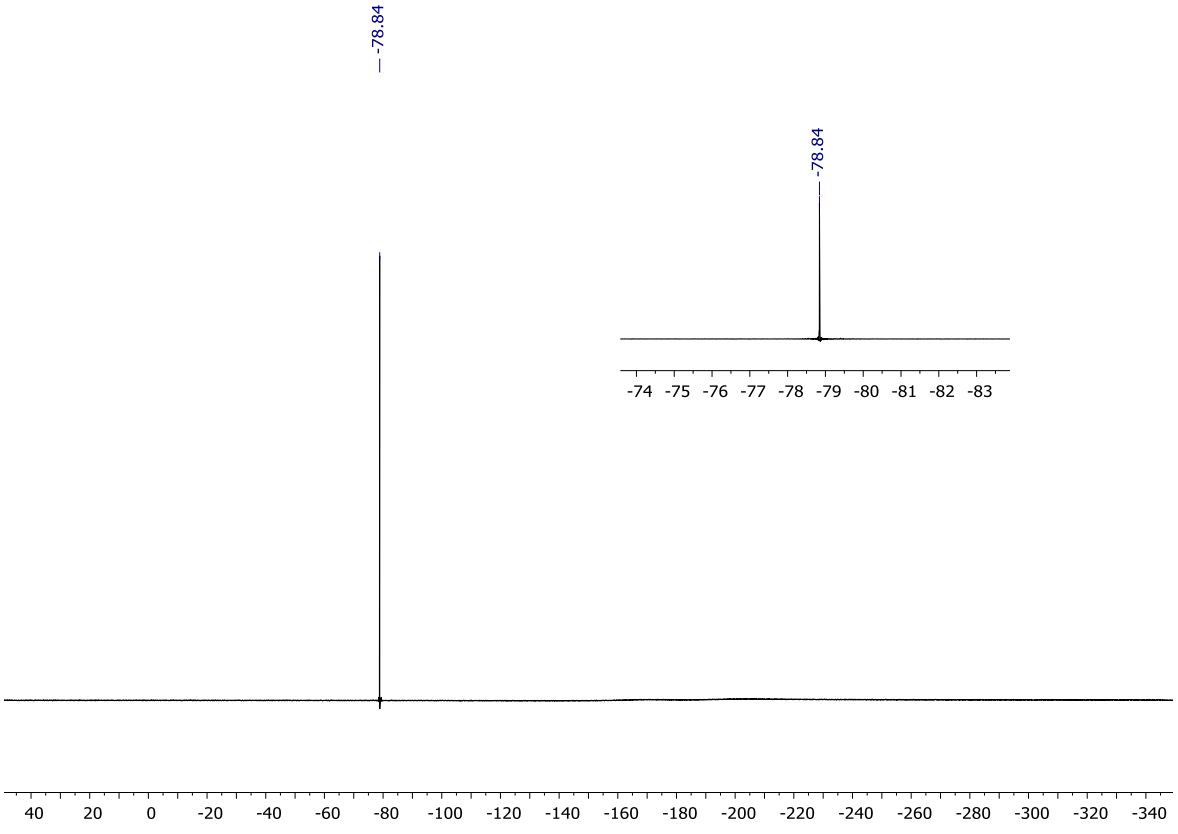

Figure **S14**: ^{19}F NMR (376 MHz, CD_2Cl_2) spectrum of **4b**[OTf]$_2$.

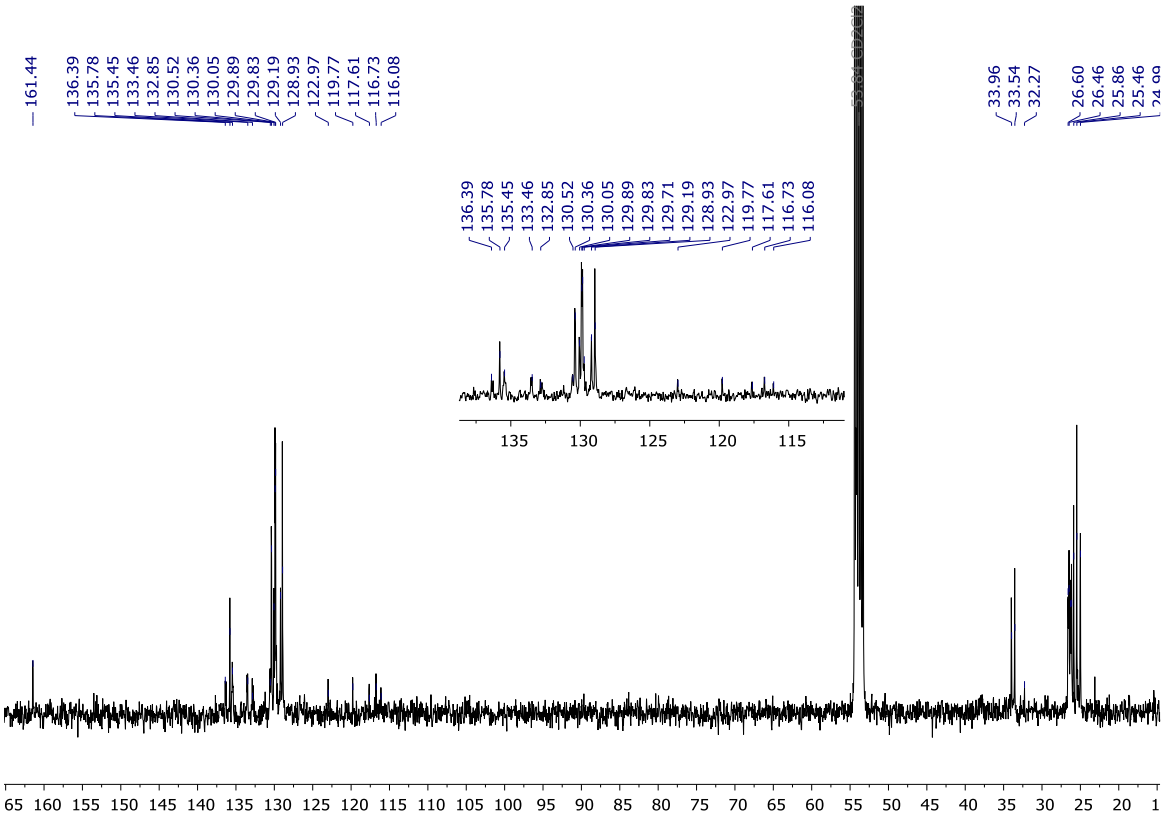

Figure **S15**: ^{13}C NMR (101 MHz, CD_2Cl_2) spectrum of **4b**[OTf]$_2$.

X-ray crystallography

Single crystals suitable for X-Ray crystal analysis were obtained by slow diffusion of vapors of pentane into a dichloromethane solution of the derivatives at rt. Single crystal data collection were performed at 150 K with an D8 VENTURE Bruker AXS diffractometer equipped with a (CMOS) PHOTON 100 detector with Mo-*K*α radiation (λ = 0.71073 Å). The structure was solved by dual-space algorithm using the *SHELXT* program[2], and then refined with full-matrix least-squares methods based on F^2 (*SHELXL*).[3] All non-hydrogen atoms were refined with anisotropic atomic displacement parameters. H atoms were finally included in their calculated positions and treated as riding on their parent atom with constrained thermal parameters.

Table S1: Crystallographic data

[2] G. M. Sheldrick, *Acta Cryst.*, **2015**, *A71*, 3-8
[3] G. M. Sheldrick, *Acta Cryst.*, **2015**, *C71*, 3-8

Compound	**4b**$[OTf]_2$	**2[OTf]**
CCDC	2001023	2001025
Formula	$C_{67}H_{74}Cl_6F_6O_6\ P_2S_2$	$C_{38}H_{28}Cl_2F_3O_3PS$
MW	1428.02	723.53
a (Å)	10.6385(8)	10.8922(12)
b (Å)	32.898(2)	11.7188(11)
c (Å)	20.1895(16)	14.7034(15)
α (°)	90	99.326(3)
β (°)	104.332(3)	102.102(4)
γ (°)	90	111.029(3)
V ($Å^3$)	6846.1(9)	1654.0(3)
Z	4	2
*D*c ($g.cm^{-3}$)	1.385	1.453
Crystal system	monoclinic	triclinic
Space group	*P* $2_1/n$	*P* -1
T (K)	150 (2)	150 (2)
Wavelength Mo-Kα (Å)	0.71073	0.71073
μ (mm^{-1})	0.425	0.363
F (000)	2968	744
θ limit (°)	3.076 to 27.484	2.194 to 27.504
Index ranges *hkl*	-13 ≤ h ≥ 13	-14 ≤ h ≥ 14
	-40 ≤ k ≥ 42	-15 ≤ k ≥ 15
	-22 ≤ l ≥ 26	-19 ≤ l ≥ 19
Reflections collected	45748	30602
Independant reflections	15656	7534
Reflections [*I*>2σ(*I*)]	13443	5685
Data / restraints / parameters	15656 / 178 / 891	7534 / 0 / 506
Goodness-of-fit on F^2	1.202	1.017
Final *R* indices [I>2σ(I)]	R1 = 0.0855	R1 = 0.00541
	wR2 = 0.2275	wR2 = 0.1348
R indices (all data)	R1= 0.0959	R1= 0.0788
	wR2= 0.2342	wR2= 0.1526
Largest diff peak and hole (e $Å^{-3}$)	1.552 and -1.263	0.542 and -0.627

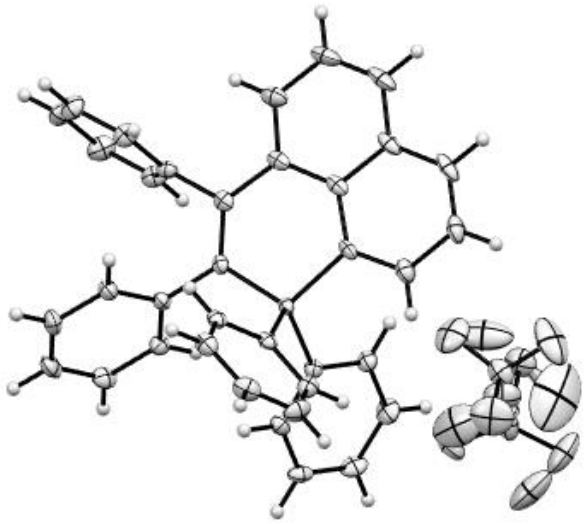

Figure S16: ORTEP representation of **2**[OTf] with 50% probability ellipsoids

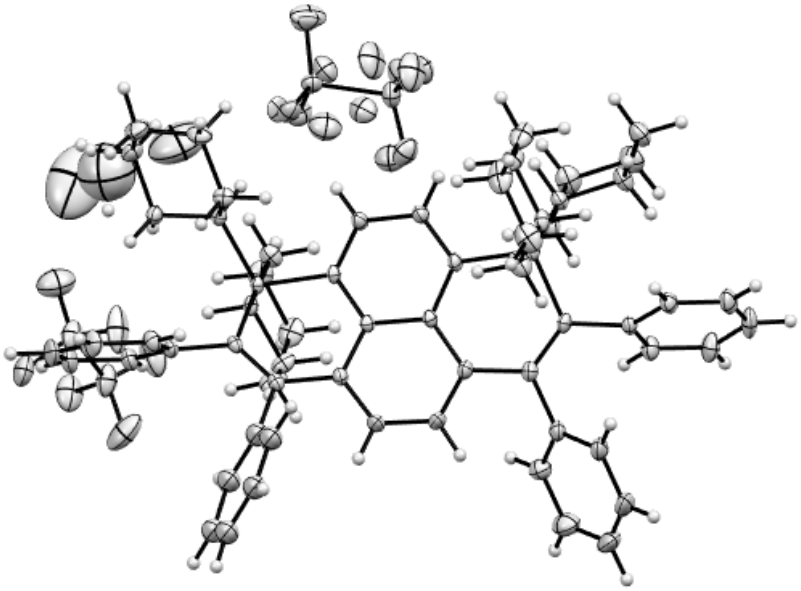

Figure S17: ORTEP representation of **4b**$[OTf]_2$ with 50% probability ellipsoids

Optical data

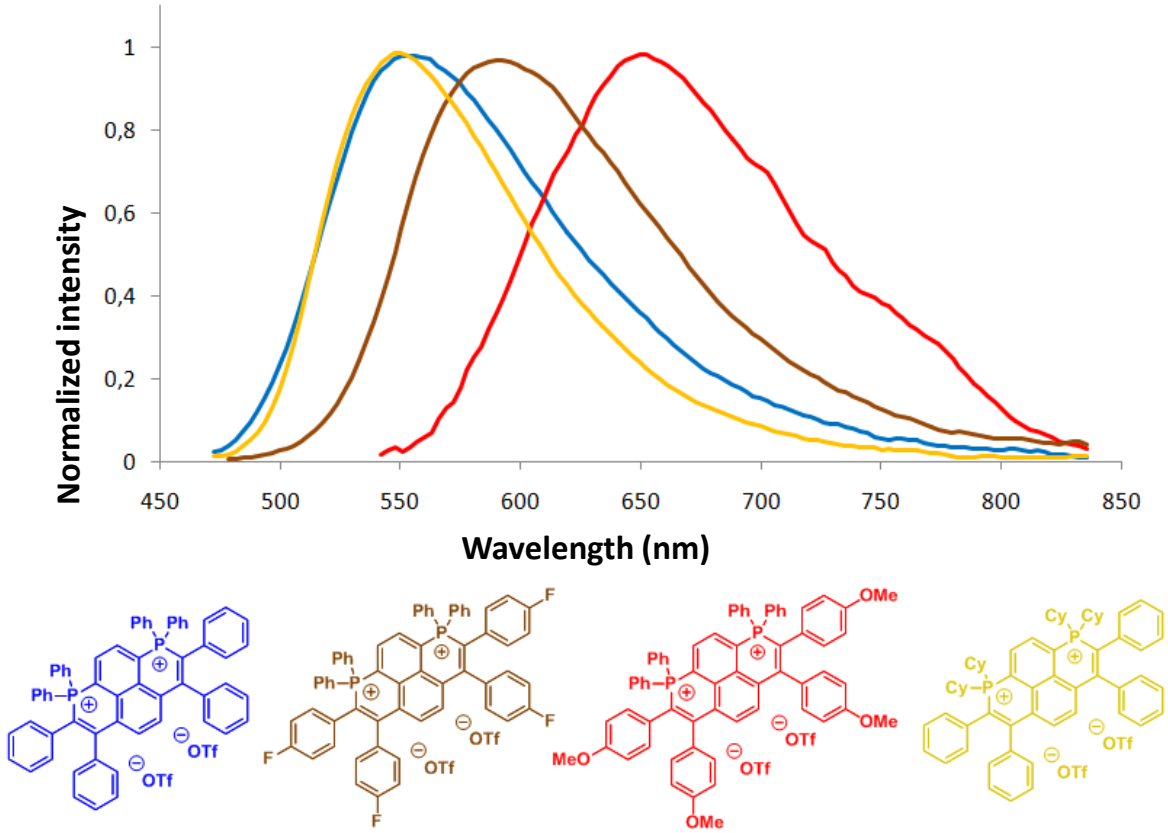

Figure S18: normalized emission in powder of **4a-d**[OTf]$_2$

Spectroelectrochemistry

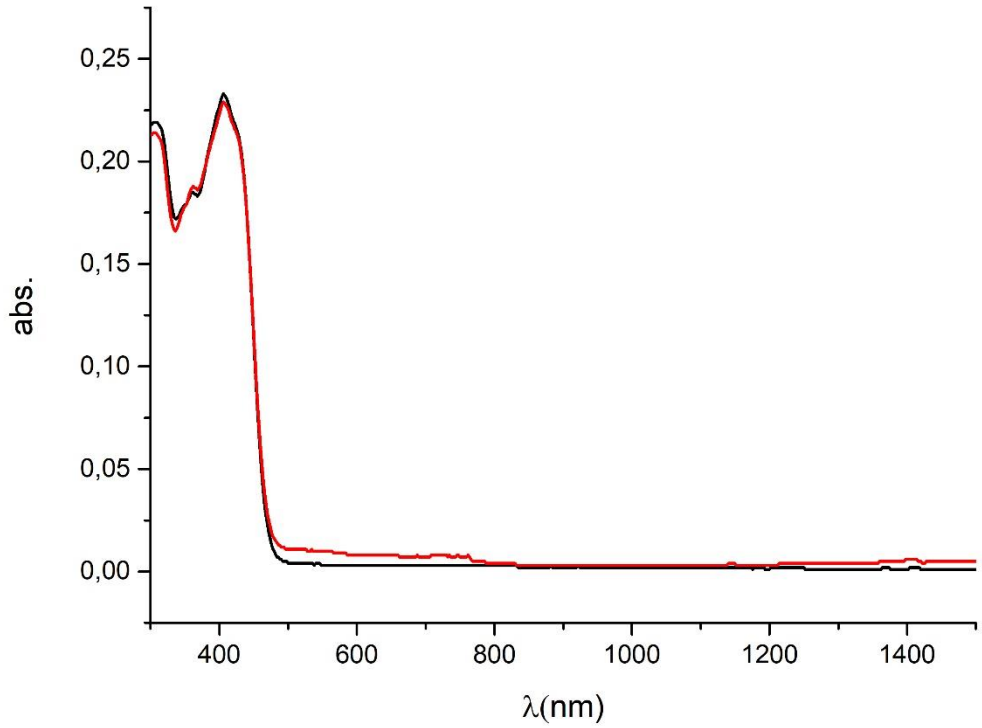

Figure S19: UV/Vis/NIR absorption spectra of **4b**$[OTf]_2$ measured before the first electrochemical reduction (black) and after returning to initial potential (red).

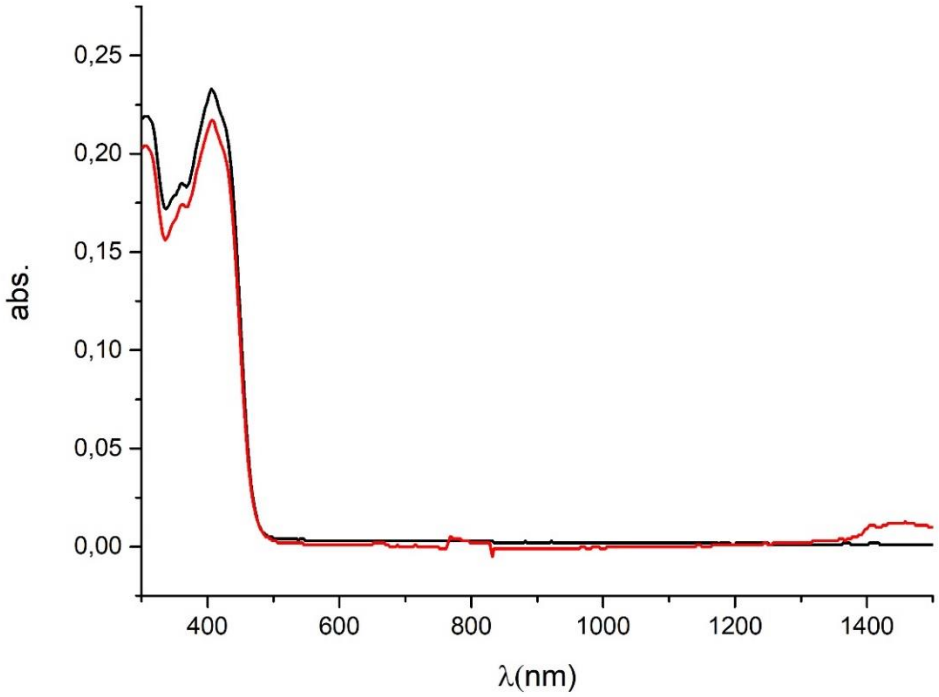

Figure S20: UV/Vis/NIR absorption spectra of **4b**[OTf]$_2$ measured before the second electrochemical reduction (black) and after returning to initial potential (red).

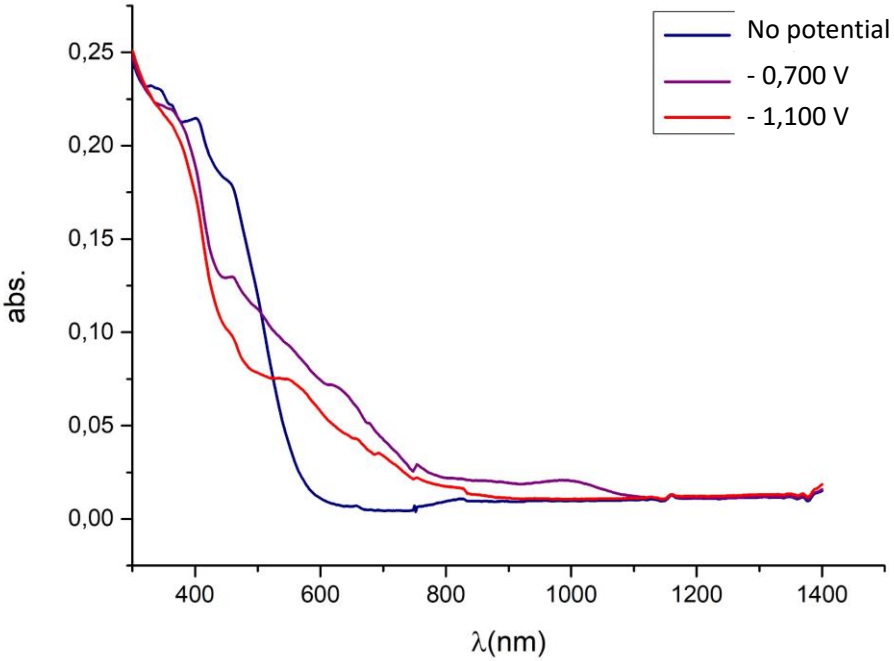

Fig S21: UV/Vis/NIR absorption spectra measured during the electrochemical reduction of **4c**$^{2+}$ (c = 5.10^{-4} M) in a solution of Bu_4NPF_6 (0.2 M) in DCM

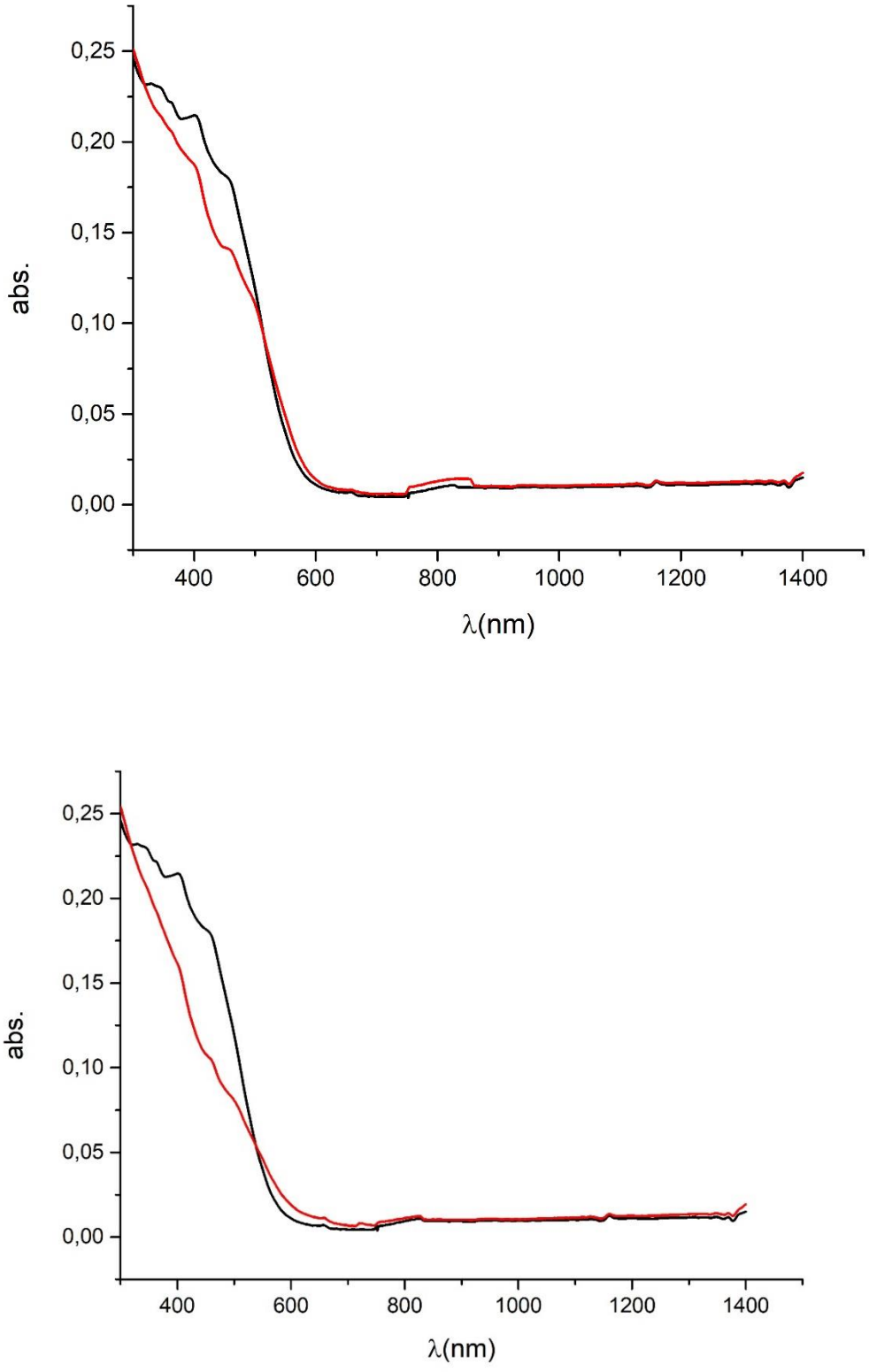

Figure S22: UV/Vis/NIR absorption spectra of **4c**$[OTf]_2$ measured before the first electrochemical reduction (black) and after returning to initial potential (red) (up) and before the second electrochemical reduction (black) and after returning to initial potential (red) (bottom).

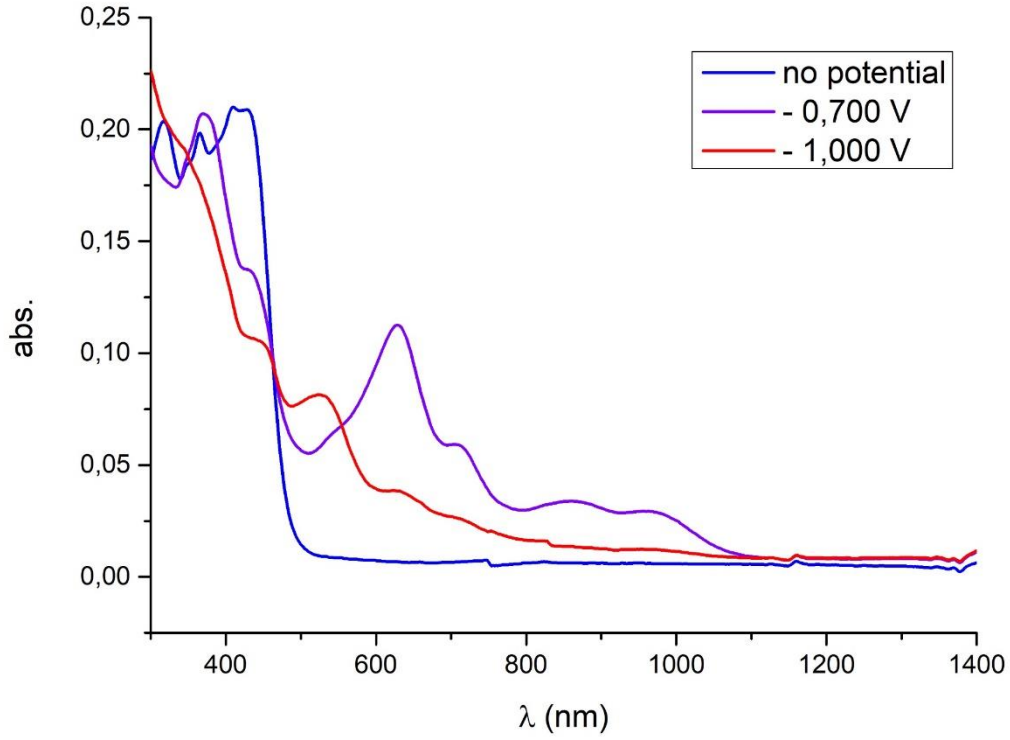

Fig S23: UV/Vis/NIR absorption spectra measured during the electrochemical reduction of **4d**$^{2+}$ (c = 5.10^{-4} M) in a solution of Bu_4NPF_6 (0.2 M) in DCM

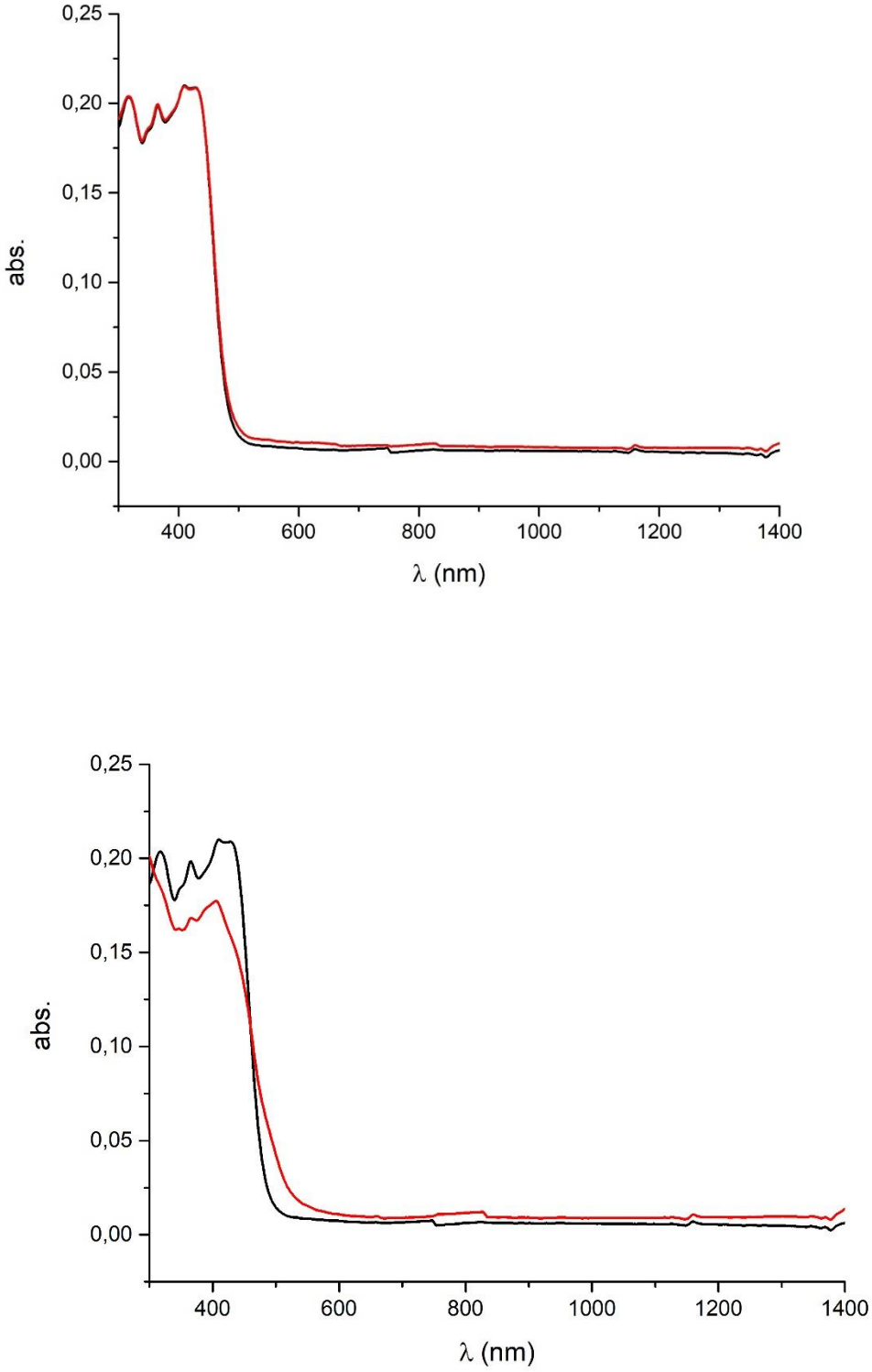

Figure S24: UV/Vis/NIR absorption spectra of **4d**$[OTf]_2$ measured before the first electrochemical reduction (black) and after returning to initial potential (red) (up) and before the second electrochemical reduction (black) and after returning to initial potential (red) (bottom).

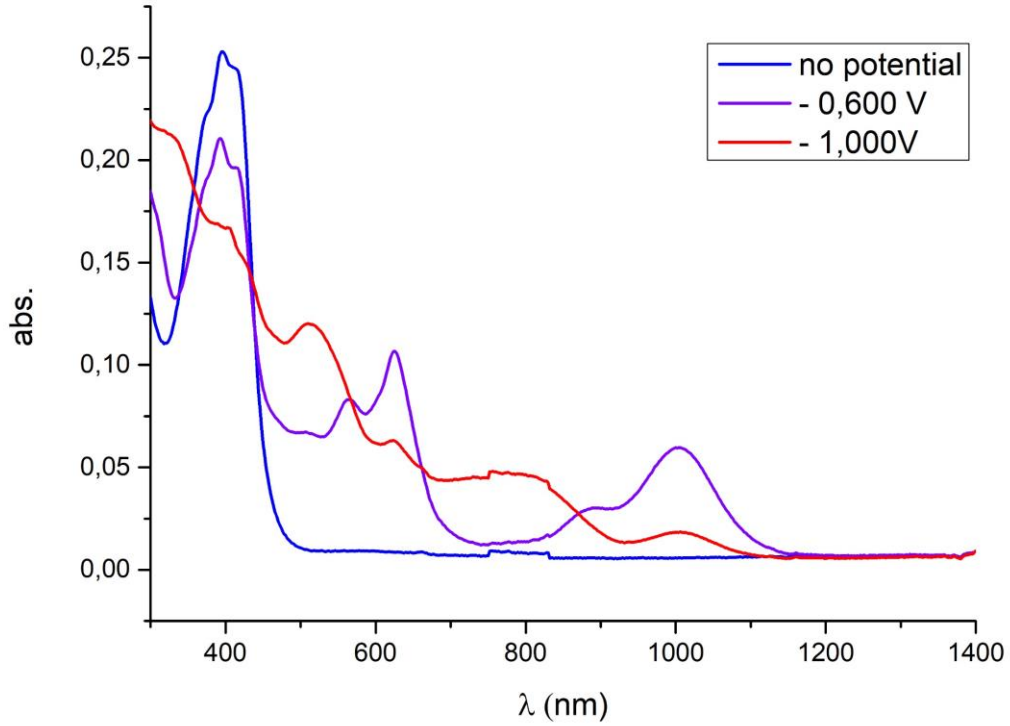

Fig S25: UV/Vis/NIR absorption spectra measured during the electrochemical reduction of $\mathbf{5}^{2+}$ (c = 5.10^{-4} M) in a solution of Bu_4NPF_6 (0.2 M) in DCM

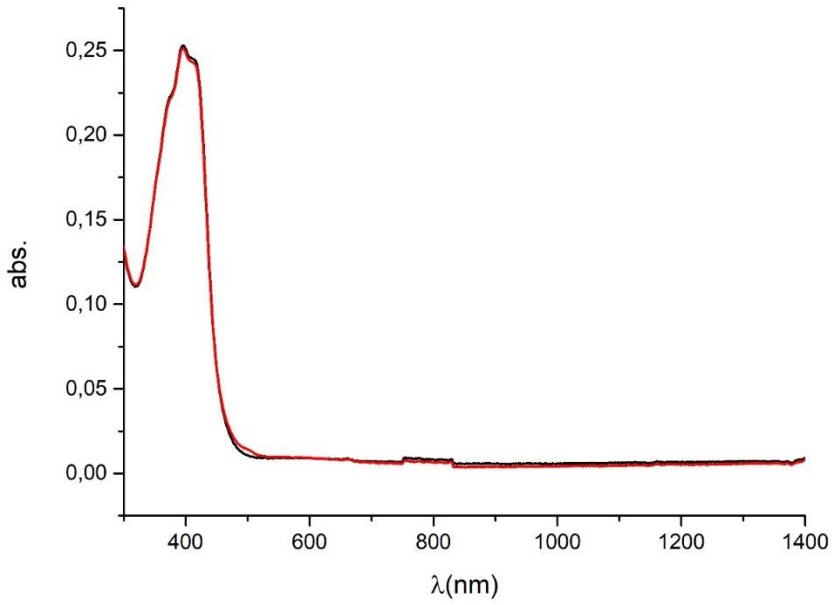

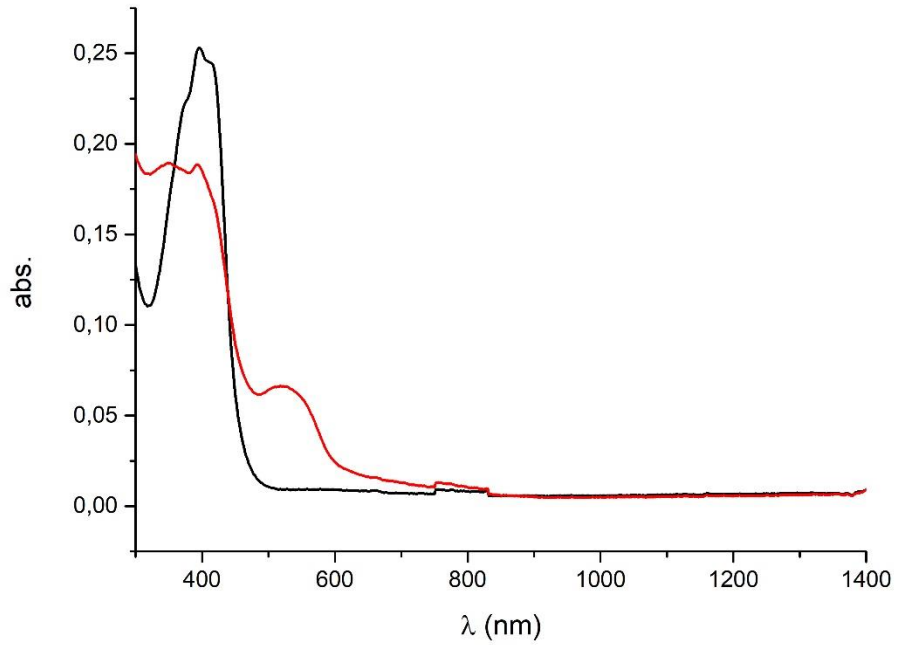

Figure S26: UV/Vis/NIR absorption spectra of **5**[OTf]$_2$ measured before the first electrochemical reduction (black) and after returning to initial potential (red) (up) and before the second electrochemical reduction (black) and after returning to initial potential (red) (bottom).

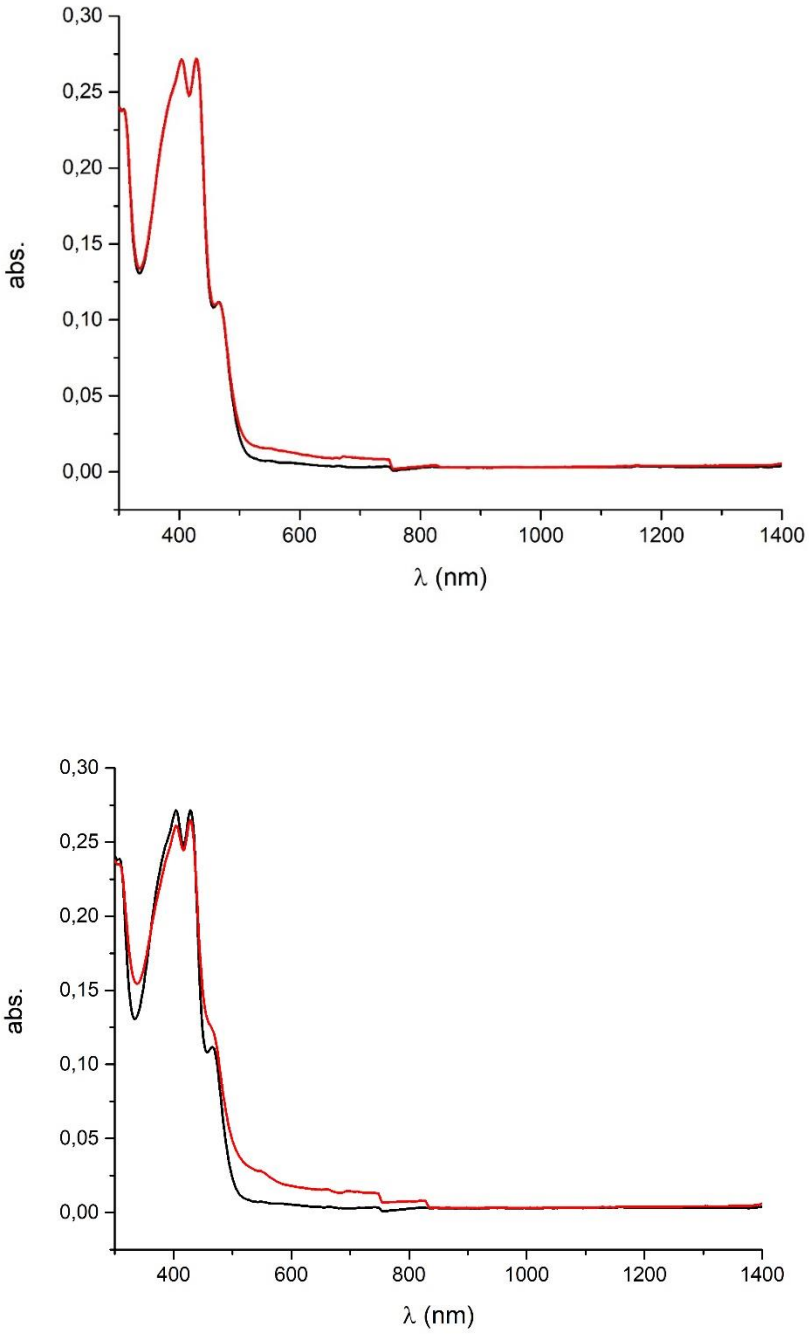

Figure S27: UV/Vis/NIR absorption spectra of **6**[OTf]$_2$ measured before the first electrochemical reduction (black) and after returning to initial potential (red) (up) and before the second electrochemical reduction (black) and after returning to initial potential (red) (bottom).

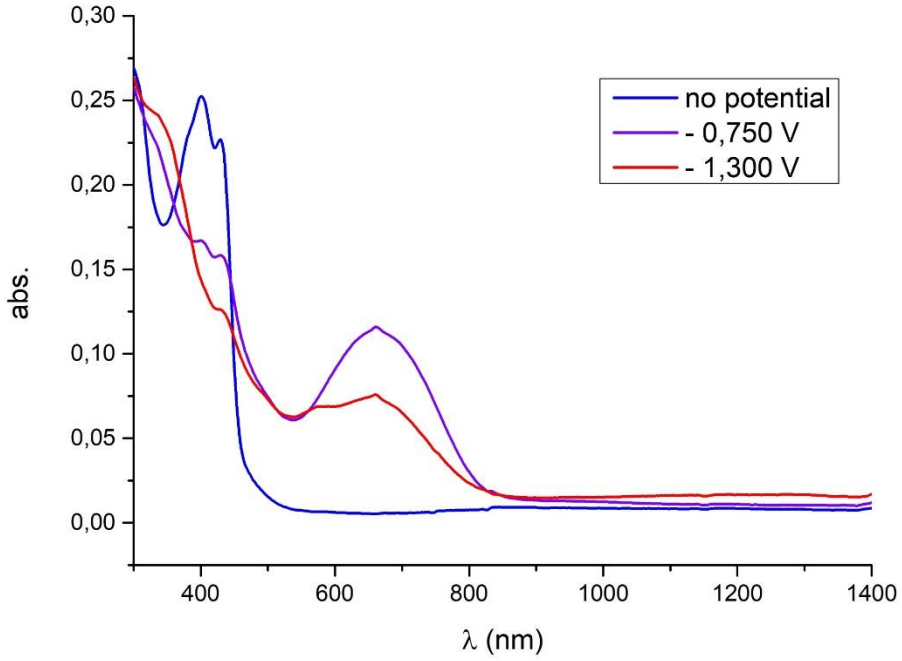

Figure S28: UV/Vis/NIR absorption spectra measured during the electrochemical reduction of $\mathbf{7}^{2+}$ (c = 5.10^{-4} M) in a solution of Bu_4NPF_6 (0.2 M) in DCM

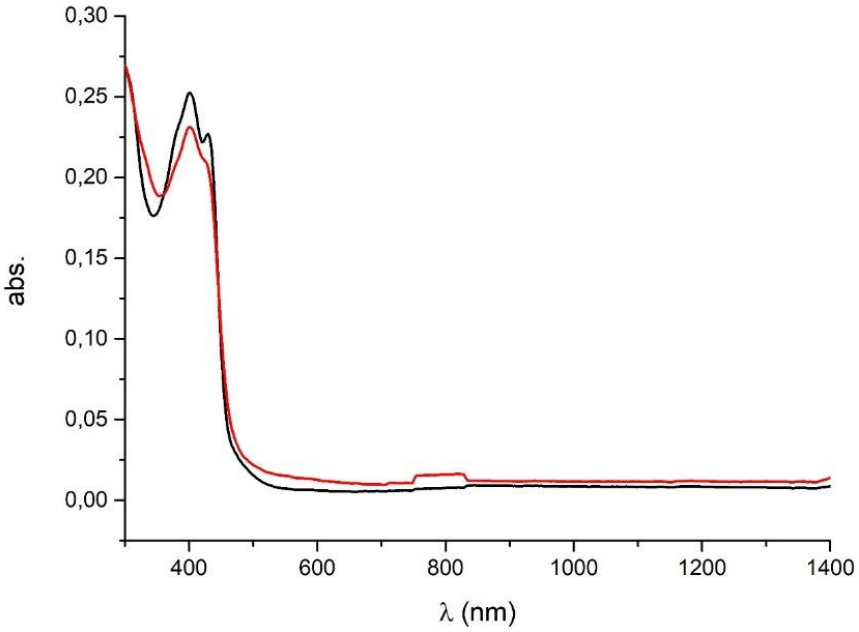

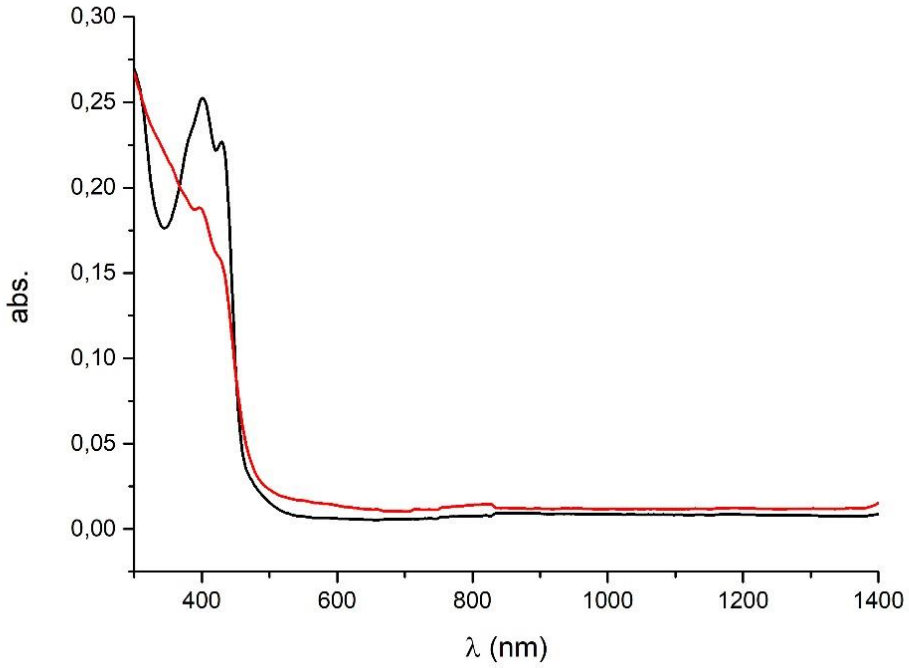

Figure S29: UV/Vis/NIR absorption spectra of **7**[OTf]$_2$ measured before the first electrochemical reduction (black) and after returning to initial potential (red) (up) and before the second electrochemical reduction (black) and after returning to initial potential (red) (bottom).

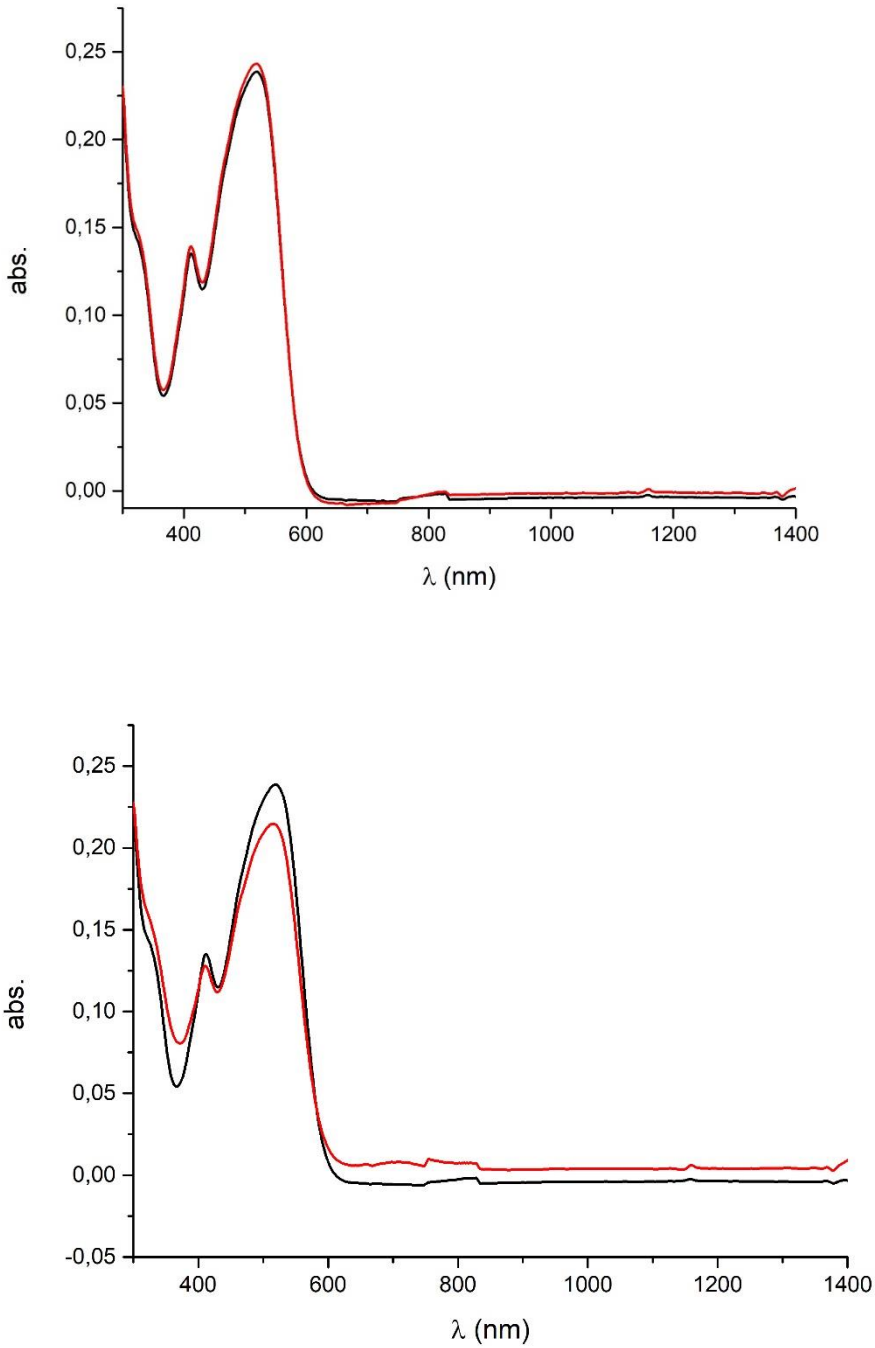

Figure S30: UV/Vis/NIR absorption spectra of **8**[OTf]$_2$ measured before the first electrochemical reduction (black) and after returning to initial potential (red) (up) and before the second electrochemical reduction (black) and after returning to initial potential (red) (bottom).

Electrofluorochromism

Electrochemistry measurements. Electrochemical measurements coupled to fluorescence were performed at room temperature using a homemade three-electrode spectroelectrochemical cell on top of an inverted optical microscope.[4] A platinum wire and an Ag|AgCl wire were used as the counter and reference electrode respectively. ITO subtrates (25-35 ohm.cm-1, 80 nm thickness, Solems) were employed as the working electrodes. Chronoamperometries were carried out with a VersaSTAT 4 (Ametek) potentiostat under VersaStudio software (Ametek). The spectroelectrochemical cell's solutions (ca. 2mL) were vigorously purged with Ar during 2 min before and at low flow rate during the measurements.

Optical measurements. Optical measurements were carried out on an inverted microscope (Ti Eclipse, Nikon) with a 40X NA 0.75 objective in a wide field epi-illumination configuration. Excitation source is made of an Hg lamp (Intensilight, Nikon) with a band pass excitation filter (BP 482nm/35 nm) and an FITC dichroic (506 nm). Emitted light is collected through a long pass emission filter (LP 520 nm). Emission fluorescence spectra were recorded with a spectrometer (SD2000, Ocean Optics) coupled to the microscope with a UV-VIS (400 µm diameter) optical fiber and a collimator placed in an intermediate image plane of the microscope. Collection area is 60 µm MFD (Mode Field Diameter) in the sample plane. Spectra are corrected from optical chain sensitivity and recorded at 1.1 spectra/s. Chronofluorogram during applied potential are obtained by the integration of the correlated fluorescence intensity in between 520 nm and 820 nm.

[4] F. Miomandre, E. Lépicier, S. Munteanu, O. Galangau, J.F. Audibert, R. Méallet-Renault, P. Audebert, and R.B. Pansu *ACS Appl. Mater. Inter.* **2011**, 3, 690–696

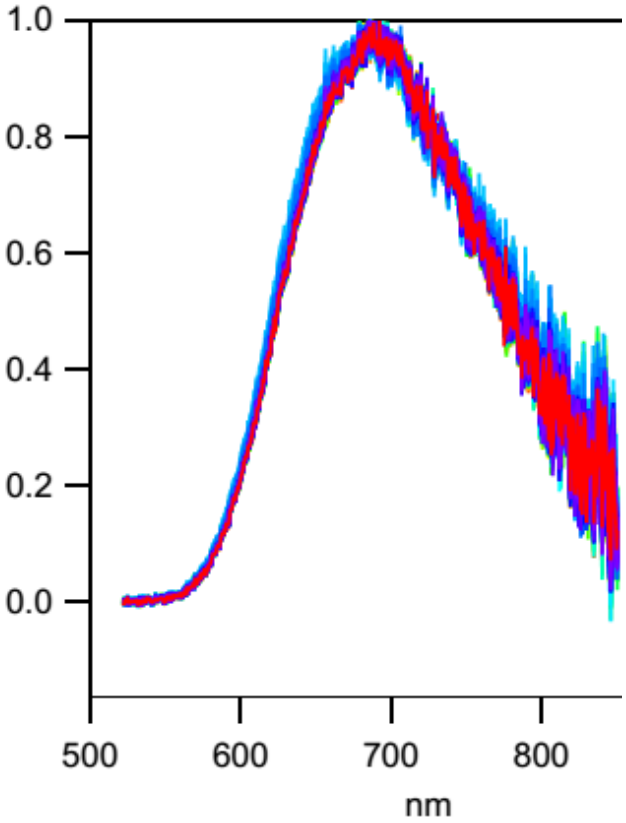

Figure S31: Overlay of emission spectra (from red to blue) along three successive potential cycles for **8**$[OTf]_2$

EPR

5 mg of compounds was dissolved in 5 ml dry degassed DCM under inert atmosphere. Then 40 mg of zinc dust was added and the mixture was stirred during 3 hours. The mixture turned to blue, then zinc is filtered with a 0.45µm PTFE syringe and the solution transferred into EPR tube. (For $\mathbf{6}^{2+}$ and $\mathbf{7}^{2+}$, Na was used as reductant instead of Zn).

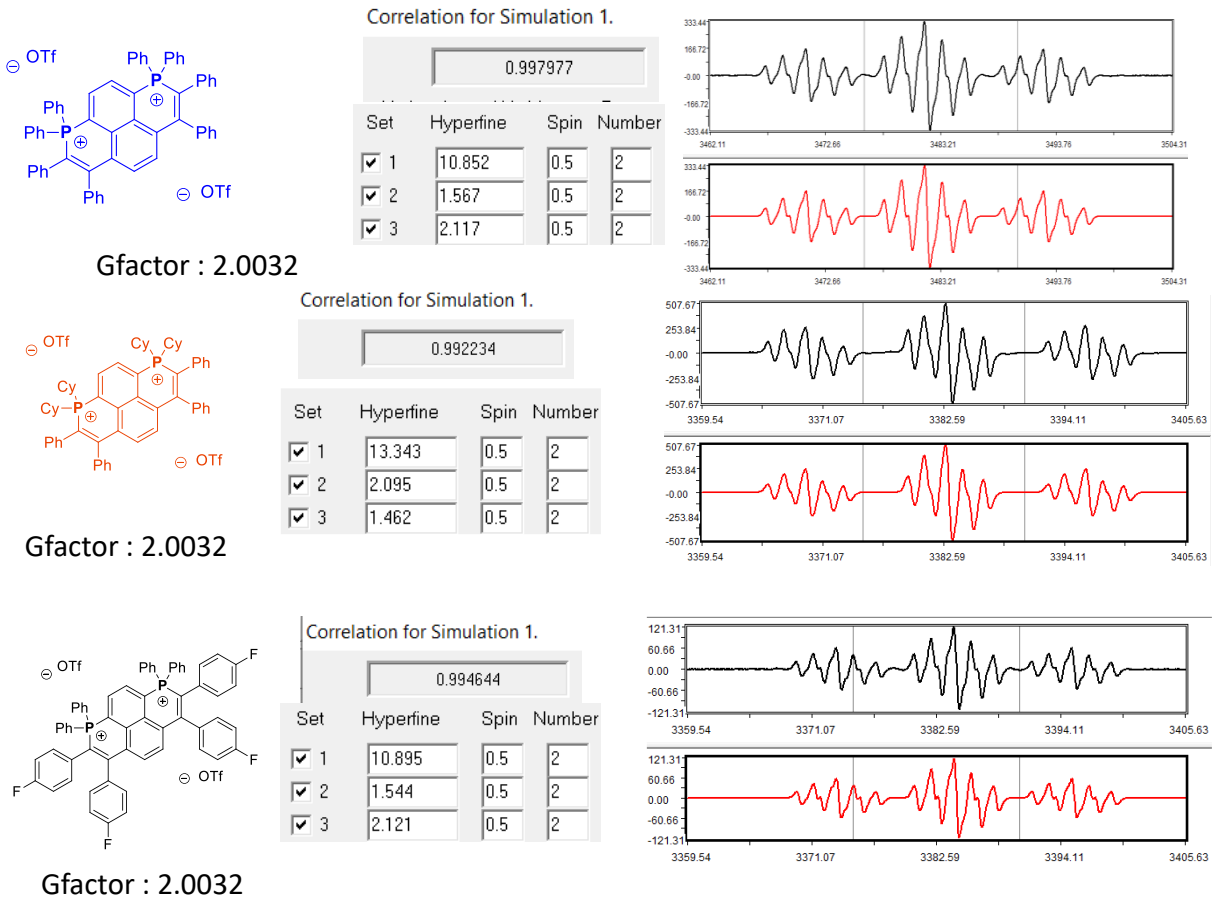

Figure S32: EPR spectrum of **4a**$[OTf]_2$ (up) **4b**$[OTf]_2$ (middle) and **4d**$[OTf]_2$ (down) upon chemical reduction in DCM at RT (black) and its simulation (red) with winsim2002.

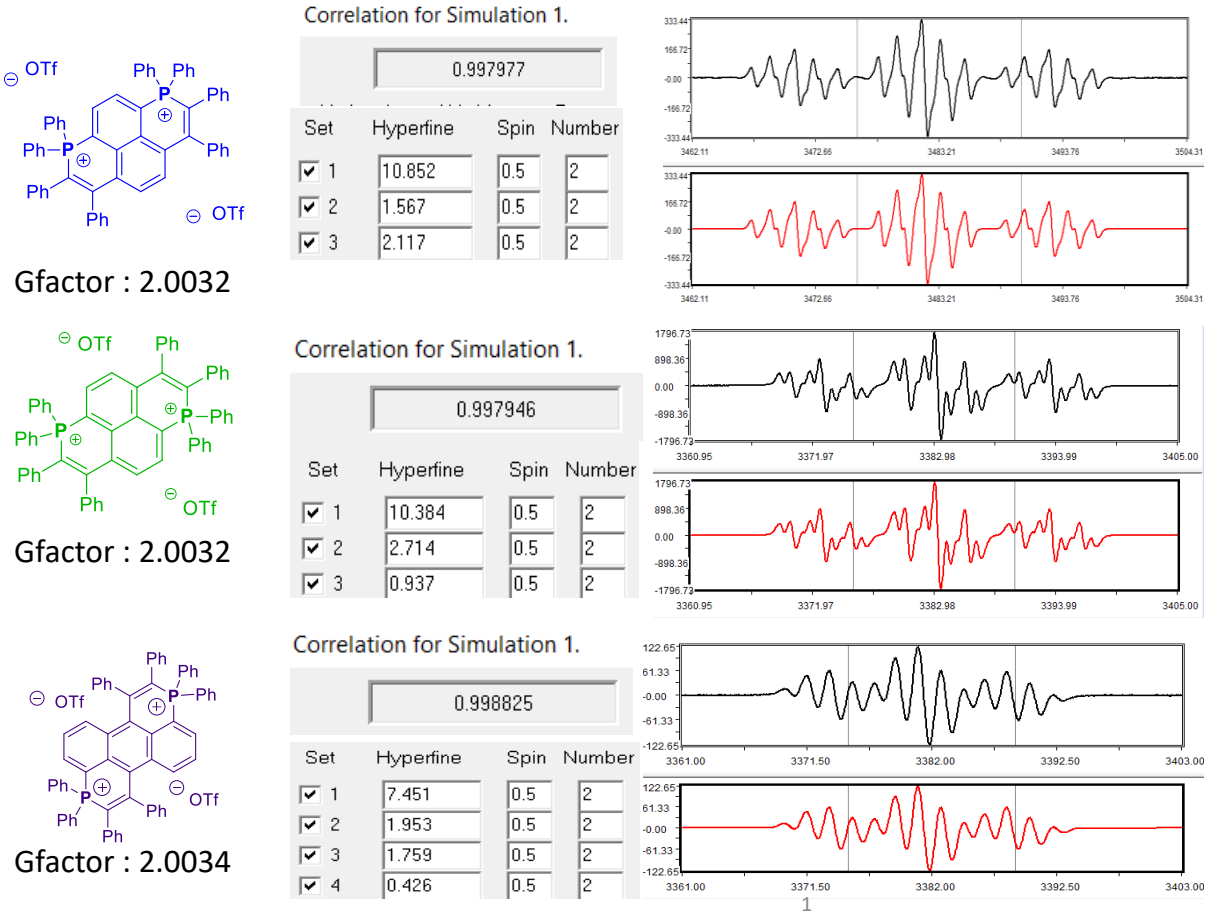

Figure S33: EPR spectrum of **5**[OTf]$_2$ (up) **6**[OTf]$_2$ (middle) and **8**[OTf]$_2$ (down) upon chemical reduction in DCM at RT (black) and its simulation (red) with winsim2002.

Theoretical Studies

All theoretical calculations have been performed with the Gaussian16 code.[5] We have applied default algorithms, parameters and convergence thresholds, but for those detailed below. The general protocol applied here follows a series of previous benchmarks performed for organic dyes and we refer the interested readers to these previous assessments for justifications and extra details.[6] First, we have performed ground-state geometry optimizations of all compounds using the M06-2X[7] functional combined with the 6-31G(d) atomic basis set for all atoms. During the force minimization process, the solvent effects (CH_2Cl_2) were accounted for using the Polarizable Continuum Model (PCM).[8] Next it was systematically checked, using an analytical determination of the nuclear Hessian, that all structures are true minima of the potential energy surface. The vertical transition energies to the lowest excited-states were determined using Time-Dependent Density Functional Theory (TD-DFT)[9] in combination with the same M06-2X functional, and a significantly larger basis set, namely 6-311+G(2d,p). During the TD-DFT calculations the solvent effects were accounted for using a combination[10] between the linear-response (LR)[11] and corrected linear-response (cLR)[12] formalisms of PCM and applying the *non-equilibrium* limit. The procedure followed to obtain estimates of the vertical fluorescence energies was very similar, with analytic optimization and vibrational frequencies of the lowest singlet states performed at the PCM(LR,*eq*)-M06-2X/6-31G(d) level, followed by determination of the emission transitions at the PCM(LR+cLR,*neq*)-M06-2X/6-311+G(2d,p) level.

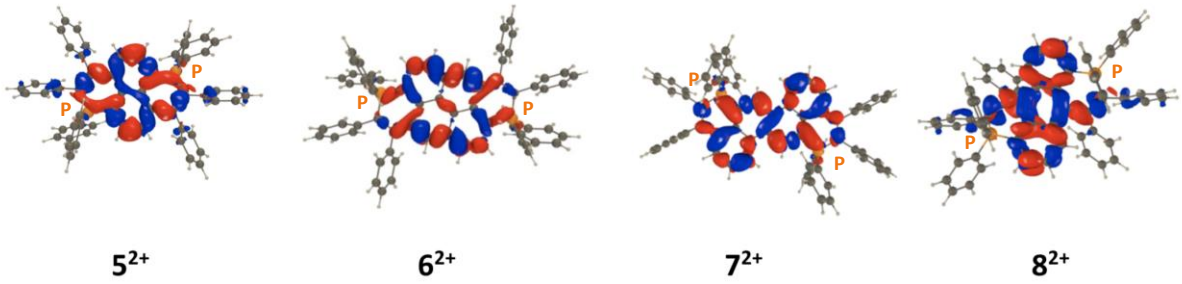

Figure S34: Electron density difference determined for **4a-8**$^{2+}$. The blue (red) lobes correspond to decrease (increase) of density upon photon absorption, respectively. A contour threshold of 8 x 10^{-4} au was used.

[5] M. J. Frisch, et al., Gaussian 16, Rev. A.03, **2016**, Gaussian Inc. Wallingford, CT.
[6] See, e.g., a) B. Le Guennic, D. Jacquemin, *Acc. Chem. Res.*, **2015**, *48*, 530; b) D. Jacquemin, I. Duchemin, X. Blase, *J. Chem. Theory Comput.*, **2015**, *11*, 5340.
[7] Y. Zhao, D. G. Truhlar, *Theor. Chem. Acc.*, **2008**, *120*, 215.
[8] J. Tomasi, B. Mennucci, R. Cammi, *Chem. Rev.* **2005**, *105*, 2999.
[9] C. Adamo, D. Jacquemin, *Chem. Soc. Rev.* **2013**, *42*, 845.
[10] P. M. Vérité, C. A. Guido, D. Jacquemin, *Phys. Chem. Chem. Phys.* **2019**, *21*, 2307.
[11] R. Cammi, B. Mennucci, *J. Chem. Phys.* **1999**, *110*, 9877.
[12] M. Caricato, B. Mennucci, J. Tomasi, F. Ingrosso, R. Cammi, S. Corni, G. Scalmani, *J. Chem. Phys.*, **2006**, *124*, 124520.

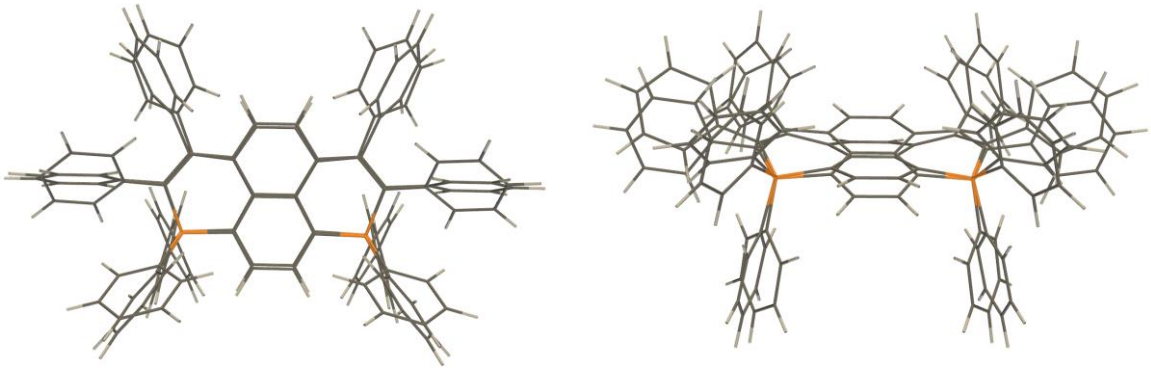

Figure S35: Two views of the superimposed ground and excited state geometries of **4a**$^{2+}$ as obtained by (TD-)DFT.

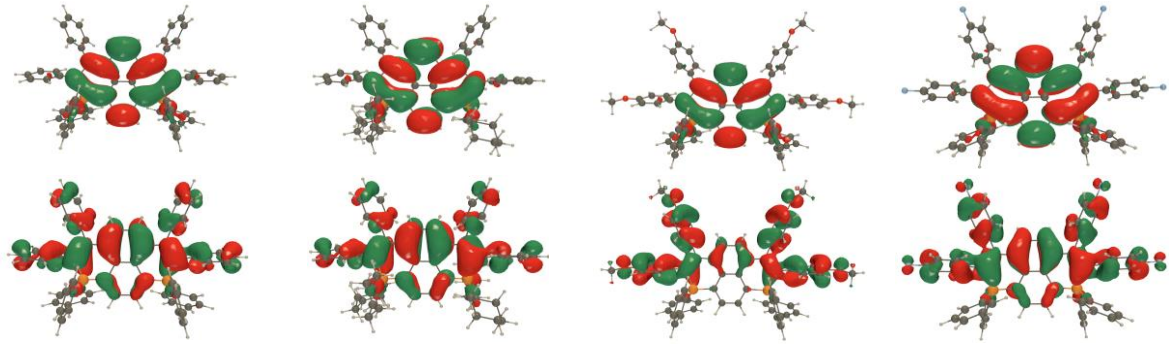

4a^{2+} **4b**$^{2+}$ **4c**$^{2+}$ **4d**$^{2+}$

Figure S36: HOMO (bottom) and LUMO (top) of **4a-d**$^{2+}$ as obtained by DFT.